JOURNAL OF GEOPHYSICAL RESEARCH, VOL. 115, D08201, doi:10.1029/2009JD013019, 2010

Detecting thin cirrus in Multiangle Imaging Spectroradiometer aerosol retrievals

Jeffrey R. Pierce,[1] Ralph A. Kahn,[2] Matt R. Davis,[3] and Jennifer M. Comstock[4]

Received 14 August 2009; revised 30 November 2009; accepted 9 December 2009; published 16 April 2010.

[1] Thin cirrus clouds (optical depth (OD) < 0.3) are often undetected by standard cloud masking in satellite aerosol retrieval algorithms. However, the Multiangle Imaging Spectroradiometer (MISR) aerosol retrieval has the potential to discriminate between the scattering phase functions of cirrus and aerosols, thus separating these components. Theoretical tests show that MISR is sensitive to cirrus OD within Max{0.05, 20%}, similar to MISR's sensitivity to aerosol OD, and MISR can distinguish between small and large crystals, even at low latitudes, where the range of scattering angles observed by MISR is smallest. Including just two cirrus components in the aerosol retrieval algorithm would capture typical MISR sensitivity to the natural range of cirrus properties; in situations where cirrus is present but the retrieval comparison space lacks these components, the retrieval tends to underestimate OD. Generally, MISR can also distinguish between cirrus and common aerosol types when the proper cirrus and aerosol optical models are included in the retrieval comparison space and total column OD is >~0.2. However, in some cases, especially at low latitudes, cirrus can be mistaken for some combinations of dust and large nonabsorbing spherical aerosols, raising a caution about retrievals in dusty marine regions when cirrus is present. Comparisons of MISR with lidar and Aerosol Robotic Network show good agreement in a majority of the cases, but situations where cirrus clouds have optical depths >0.15 and are horizontally inhomogeneous on spatial scales shorter than ~50 km pose difficulties for cirrus retrieval using the MISR standard aerosol algorithm.

Citation: Pierce, J. R., R. A. Kahn, M. R. Davis, and J. M. Comstock (2010), Detecting thin cirrus in Multiangle Imaging Spectroradiometer aerosol retrievals, *J. Geophys. Res.*, *115*, D08201, doi:10.1029/2009JD013019.

1. Introduction

[2] Thin cirrus clouds, classified here as cirrus with optical depths (ODs) between about 0.03 and 0.3 [*Sassen and Cho*, 1992], are common in the atmosphere and may dominate the cirrus coverage globally [*Comstock et al.*, 2002]. In addition to being important to the radiative budget of the atmosphere [*Forster et al.*, 2007], thin cirrus can contribute significantly to the radiances measured from passive Earth-observing-satellite instruments; however, it can be difficult to uniquely identify the amount they contribute to these radiances [*Kahn et al.*, 2001]. Principal Earth-observing-satellite applications affected by thin cirrus are the measurement of aerosol optical depth (AOD) and aerosol physical properties (e.g., shape, size, and single-scattering albedo) from passive imaging instruments [*Kaufman et al.*, 2005]. For most passive imaging instruments, including the Multiangle Imaging Spectroradiometer (MISR) on board NASA's Earth Observing System (EOS) Terra satellite, the ability to identify and mask cloudy pixels with standard methods when retrieving aerosol parameters begins to break down when cloud optical depths fall below about 0.3 in the nadir view and around 0.1 for the steepest forward-viewing MISR camera [*Zhao and Di Girolamo*, 2004; *Zhao*, 2006]. This means that when present, thin cirrus might actually contribute to the retrieved aerosol products, aliasing the results. However, if MISR is able to identify thin cirrus and possibly constrain their physical properties, there may be improvements in both aerosol products and our understanding of the nature of thin cirrus.

[3] Recently, progress has been made in determining thin cirrus coverage statistics, particularly in the tropics. *Comstock et al.* [2002] and *Immler et al.* [2007] both present statistics of cirrus optical depth from ground-based lidar in tropical locations, and both show a preponderance of thin cirrus. *Dessler and Yang* [2003], *Dessler et al.* [2006], and *Kahn et al.* [2008] used the Moderate Resolution Imaging Spectrometer (MODIS) 1.375 μm band designed for cirrus detection, the Geoscience Laser Altimeter System, and the Atmospheric Infrared Sounder satellite instruments, respectively, to measure tropical thin cirrus coverage. Even with these advancements, large uncertainties remain in both the macroscale and microscale property climatologies of thin cirrus, as well as how they contribute to clear-sky top-of-

[1]Department of Physics and Atmospheric Science, Dalhousie University, Halifax, Nova Scotia, Canada.
[2]Laboratory for Atmospheres, NASA Goddard Space Flight Center, Greenbelt, Maryland, USA.
[3]Science Systems and Applications, Inc., Lanham, Maryland, USA.
[4]Pacific Northwest National Laboratory, Richland, Washington, USA.

0148-0227/10/2009JD013019

atmosphere (TOA) radiances measured by MISR and other remote-sensing instruments.

[4] MISR views Earth with four spectral bands, centered at 446, 558, 672, and 867 nm, from each of nine different viewing angles, 70.5°, 60.0°, 45.6°, and 26.1° in both the forward and aft directions along the flight path, as well as nadir. MISR was launched into polar orbit and has been operational since early 2000, viewing Earth with a ~360 km wide swath and a spatial resolution of 275 m to 1 km, depending on channel and instrument viewing mode. Zonal coverage is completed every 9 days at the equator and 2 days near the poles [*Diner et al.*, 1998]. The unique combination of multispectral and multiangle information from MISR yields information on both extensive (optical depth) and intensive (size, shape, and single-scattering albedo) aerosol properties. Aerosol retrievals are performed by fitting the MISR radiances using the spectrally dependent scattering phase functions of typical atmospheric aerosols [*Martonchik et al.*, 1998; *Kahn et al.*, 2001]. *McFarlane et al.* [2005] and *McFarlane and Marchand* [2008] have successfully developed a technique for retrieving opaque cirrus properties using MISR radiances along with the 2.13 μm MODIS band.

[5] If the spectrally dependent scattering phase functions of various ice-crystal habits are known, these phase functions can be incorporated with the aerosol phase functions in the radiance fit, and the cirrus and aerosol contributions might be separated, depending on uniqueness. As part of prelaunch theoretical sensitivity studies, *Kahn et al.* [2001] performed initial tests of the ability to resolve thin cirrus in MISR aerosol retrievals. Using a standard ice-crystal phase function available at the time [*Mishchenko et al.*, 1996], they found that in principle, the retrieval could distinguish thin cirrus from aerosols if the total column optical depth is greater than about 0.2 and the cirrus contribution is more than 20%. The ability to distinguish between aerosol types was reduced by the presence of cirrus, but the sensitivity to total aerosol optical depth was maintained. A limitation of these tests was that only a single ice-crystal phase function was used for both the retrieval comparison space and the assumed test atmosphere.

[6] However, ice-crystal phase functions in the real atmosphere are uncertain because crystals exist in many shapes and sizes [*Baum et al.*, 2005a] that depend on the environment in which they are formed. The scattering phase functions depend particularly on crystal shape [*Zhang et al.*, 2004]. With the MISR aerosol retrieval method, if the assumed phase functions do not closely match the phase functions of cirrus in the atmosphere, the ability to resolve cirrus shown by *Kahn et al.* [2001] would be reduced. Fortunately, progress has been made in understanding ice-crystal scattering properties; in addition to hexagonal crystal phase functions often used to represent thin cirrus [*Takano and Liou*, 1989], *Baum et al.* [2005a, 2005b] present a suite of ice-crystal mixtures and corresponding phase functions derived from extensive tropical and midlatitude field measurements. Several of these ice-crystal mixtures are likely common in tropical and midlatitude thin cirrus and may be useful for decoupling thin cirrus and aerosols in MISR aerosol retrievals.

[7] In this paper, we greatly expand on the MISR thin cirrus theoretical sensitivity tests first presented by *Kahn et al.* [2001] by exploring how mismatches between the ice-crystal type (shape and size) assumed in the retrieval algorithm and those actually in the atmosphere affect the retrieval results. Similar theoretical sensitivity tests have been used previously to determine the sensitivity of MISR to particle sphericity/dust [*Kahn et al.*, 1997; *Kalashnikova and Kahn*, 2006], spherical particle size and single-scattering albedo [*Kahn et al.*, 1998; *Chen et al.*, 2008], and particle mixtures [*Kahn et al.*, 2001]. In the theoretical tests presented here, we will ask the following questions:

[8] 1. Which combinations of ice-crystal type assumed in the algorithm and actually in the atmosphere will yield acceptable retrievals? How sensitive is MISR to cirrus optical depth in these cases?

[9] 2. Are there a small number of ice-crystal types that can generally represent all crystal types tested here, within the limits of MISR retrieval sensitivity? This could provide a practical way to include cirrus in a future version of the MISR standard aerosol retrieval algorithm.

[10] 3. Under what cirrus type, aerosol type, and total column optical depth conditions, and to what degree, is the algorithm likely to falsely identify cirrus as aerosol?

[11] 4. Under what cirrus type, aerosol type, and total column optical depth conditions, and to what degree, is the algorithm likely to falsely identify aerosol as cirrus?

[12] Following the theoretical sensitivity tests, we explore MISR's ability to retrieve cirrus in the real atmosphere using ground-based lidar measurements coincident with MISR flyovers. These comparisons allow us to test the theoretical study results.

[13] In the following section, we describe the ice-crystal models used here to assess MISR sensitivity to cirrus in aerosol retrievals and present the theoretical sensitivity study results. Coincident MISR and ground-based lidar cirrus retrievals as well as coincident MISR and Aerosol Robotic Network (AERONET) optical depth retrievals for natural cases are compared in section 3. Conclusions follow in section 4.

2. Theoretical Multiangle Imaging Spectroradiometer (MISR) Sensitivity to Thin Cirrus

2.1. Ice-Crystal and Aerosol Types

[14] The ice-crystal and aerosol types used in this paper are shown in Table 1. Included are 18 ice-crystal types based on observations collected by *Baum et al.* [2005a]. *Baum et al.* [2005b] describe the bulk scattering properties derived from the observations. The data for MISR wavelengths are available (http://www.ssec.wisc.edu/~baum/Cirrus/MISR_Models.html). These crystal types represent 18 possible ice-crystal size distributions found in the atmosphere with effective diameters that vary from 10 to 180 μm. (Effective diameter is defined as 1.5 times the ratio of the crystal volume to the average projected area, assuming particles are randomly oriented.) The smallest crystals tend to be shaped like droxtals, which have 20 facets and are designed to represent small quasi-spherical particles [*Zhang et al.*, 2004]. These crystals are formed at very low temperatures and water vapor concentrations, whereas the larger crystals are represented by mixtures of shapes that depend on their sizes (http://www.ssec.wisc.edu/~baum/Cirrus/MISR_Models.html). A nineteenth ice-crystal type is that of solid hexagonal

crystals with L/D of 2 and an effective diameter of 40 μm, a typical habit for representing cirrus clouds [*Takano and Liou*, 1989; *Macke et al.*, 1996].

[15] The phase functions for four of the Baum crystal types as well as the Hex $L/D = 2$ at the MISR red-band wavelength are plotted in Figure 1a. Figure 1a also shows the scattering angles (dotted lines) of the nine MISR cameras when Terra is located above 10°S during the equinox. Differences between the plotted phase functions are dominated by crystal shape rather than size. (These crystals are all much larger than the MISR wavelengths, so size differences make only minor changes to the phase functions.) The Baum D_e = 10 μm crystal type, dominated by the droxtal geometry, is the only one of these crystal types to have an increasing phase function with scattering angle across the range of MISR scattering angles. The Baum D_e = 100 and 160 μm and Hex $L/D = 2$ all have similarly shaped phase functions across these scattering angles. These similarities are due to crystals with diameters between 60 and 2500 μm in the *Baum et al.* [2005a] climatology all being dominated by hexagonal structures (solid columns, hollow columns and plates). Evaluated at typical MISR equatorial scattering angles, the phase function for the Baum D_e = 40 μm ice-crystal type falls between these two regimes, as it is a mixture of droxtals and hexagonal structures. These phase functions are consistent with the droxtals and various hexagonal structures presented by *Zhang et al.* [2004] and *Macke et al.* [1996]. It is important to note that most of the ice crystals included in these models have smooth surfaces and no air bubbles. As such features might affect the scattering phase functions for remote sensing applications, there is a need to develop a comprehensive set of natural-ice-crystal optical analogs that takes these factors into account [*Yang et al.*, 2008].

[16] Table 1 also shows seven aerosol types. Included are four sizes of nonabsorbing spheres, two small absorbing spheres, and two dust types. Figure 1b shows the phase functions of three nonabsorbing spheres along with three ice-crystal types. The phase functions of the spheres are distinct from those of the ice crystals; however, it is possible that some combinations of spheres may produce an effective phase function similar to an ice-crystal type. Figure 1c shows the phase functions of the two dust particle types, the largest nonabsorbing sphere, and the same three ice-crystal types. Combinations of aerosols and ice crystals will be explored in sections 2.4 and 2.5.

2.2. Radiative Transfer Simulations and the MISR Aerosol Research Retrieval

[17] In these sensitivity tests, we assess our ability to retrieve cirrus and aerosol properties from simulated MISR "observed" radiances for preselected, simulated atmospheres. TOA equivalent reflectances at MISR wavelengths and angles are calculated for these simulated atmospheres using a radiative transfer code developed by the MISR team [*Martonchik et al.*, 1998] based on the matrix operator method [*Grant and Hunt*, 1968]. A specified optical depth of an ice-crystal type or aerosol type from Table 1 is included in each atmosphere. A cloud-free, Rayleigh scattering atmosphere over a Fresnel reflecting dark water surface with 1 atm surface pressure and 2.5 m s^{-1} wind speed is specified. These assumptions represent natural, good, but not ideal observing conditions [*Kahn et al.*, 1997, 1998, 2001; *Kalashnikova and Kahn*, 2006; *Chen et al.*, 2008]. This simulated atmosphere is placed at 10°S during the equinox, where the range of MISR scattering angles is close to its minimum value. The small range of MISR scattering angles reduces MISR sensitivity [*Kahn et al.*, 2001], but due to the frequent occurrence of cirrus clouds in the tropics, we chose to do the sensitivity tests here; we expect MISR to have *higher* sensitivity to cirrus and aerosols at higher latitudes. In these tests, we assume that aerosols are distributed in the first 10 km of the atmosphere and cirrus are confined to a layer between 10 and 11 km. The assumed vertical distribution matters most for absorbing species, such as soot and smoke. In general, absorbing aerosols tend to concentrate below thin cirrus, so the exact height of the cirrus does not matter greatly, provided that it is assumed to be above the absorbing aerosols.

[18] The ability of MISR to determine aerosol and cirrus properties in these simulated atmospheres is tested using the MISR aerosol research retrieval algorithm [*Kahn et al.*, 2001]. Up to four component particles (cirrus or aerosol) are aggregated into "mixing groups" (to be defined in the following subsections). TOA radiances are calculated for atmospheres having total cirrus/aerosol mixture optical depths ranging from 0 to 1 in increments of 0.05, with fractions of each cirrus or aerosol component ranging from 0 to 1 (also in increments of 0.05). The same radiative transfer code and atmospheric assumptions for the simulated atmosphere described above are used here.

[19] To test whether a given mixture of aerosols/cirrus in the research retrieval is an acceptable fit to the simulated atmosphere, we use the χ^2 method that is described in detail by *Kahn et al.* [1997, 1998, 2001]. Three variants of this statistic, χ^2_{abs}, χ^2_{geon}, and χ^2_{spec}, compare the absolute reflectances, reflectance ratios normalized to one view angle, and reflectance ratios normalized to one wavelength, respectively, between the atmosphere and the comparison space (i.e., each aerosol/cirrus mixture tested in the research retrieval). Each test variable is normalized by the number of channels and cameras used. The reflectances of up to four-component mixtures are considered indistinguishable from those of the atmosphere if the maximum of the three χ^2 test variables,

$$\chi^2_{max3} = \mathrm{Max}\left\{\chi^2_{abs}, \chi^2_{geon}, \chi^2_{spec}\right\}, \quad (1)$$

is less than a chosen constraint. $\chi^2_{max3} < 1$ means the average difference between the atmosphere and a comparison mixture is less than the associated measurement error. The smaller the number of aerosol/cirrus mixtures and optical depths that produce acceptable matches, the greater is the measurement sensitivity.

2.3. MISR Theoretical Sensitivity to Ice-Crystal Type and Optical Depth

[20] In this section we ask the following questions:

[21] 1. How sensitive is MISR to different ice-crystal types at low latitudes when the atmosphere contains only cirrus?

[22] 2. How sensitive is MISR to cirrus optical depth in these cases?

[23] 3. Is there a small number of ice-crystal types that can generally represent all the crystal types tested here, to the degree that MISR can make crystal shape distinctions?

Table 1. Properties of Ice-Crystal and Aerosol Types Used in This Paper[a]

Type	Distribution Type	r_1(μm)	r_2(μm)	r_c(μm)	σ	r_e(μm)	SSA 446 nm	SSA 558 nm	SSA 672 nm	SSA 866 nm
					Baum D_e = 10 μm					
Cirrus	Gamma	2	9500	NA	NA	5	1.000	1.000	1.000	1.000
					Baum D_e = 20 μm					
Cirrus	Gamma	2	9500	NA	NA	10	1.000	1.000	1.000	1.000
					Baum D_e = 30 μm					
Cirrus	Gamma	2	9500	NA	NA	15	1.000	1.000	1.000	1.000
					Baum D_e = 40 μm					
Cirrus	Gamma	2	9500	NA	NA	20	1.000	1.000	1.000	1.000
					Baum D_e = 50 μm					
Cirrus	Gamma	2	9500	NA	NA	25	1.000	1.000	1.000	1.000
					Baum D_e = 60 μm					
Cirrus	Gamma	2	9500	NA	NA	30	1.000	1.000	1.000	1.000
					Baum D_e = 70 μm					
Cirrus	Gamma	2	9500	NA	NA	35	1.000	1.000	1.000	1.000
					Baum D_e = 80 μm					
Cirrus	Gamma	2	9500	NA	NA	40	1.000	1.000	1.000	1.000
					Baum D_e = 90 μm					
Cirrus	Gamma	2	9500	NA	NA	45	1.000	1.000	1.000	1.000
					Baum D_e = 100 μm					
Cirrus	Gamma	2	9500	NA	NA	50	1.000	1.000	1.000	1.000
					Baum D_e = 110 μm					
Cirrus	Gamma	2	9500	NA	NA	55	1.000	1.000	1.000	1.000
					Baum D_e = 120 μm					
Cirrus	Gamma	2	9500	NA	NA	60	1.000	1.000	1.000	1.000
					Baum D_e = 130 μm					
Cirrus	Gamma	2	9500	NA	NA	65	1.000	1.000	1.000	1.000
					Baum D_e = 140 μm					
Cirrus	Gamma	2	9500	NA	NA	70	1.000	1.000	1.000	1.000
					Baum D_e = 150 μm					
Cirrus	Gamma	2	9500	NA	NA	75	1.000	1.000	1.000	1.000
					Baum D_e = 160 μm					
Cirrus	Gamma	2	9500	NA	NA	80	1.000	1.000	1.000	1.000
					Baum D_e = 170 μm					
Cirrus	Gamma	2	9500	NA	NA	85	1.000	1.000	1.000	1.000
					Baum D_e = 180 μm					
Cirrus	Gamma	2	9500	NA	NA	90	1.000	1.000	1.000	1.000
					Hex, L/D = 2					
Cirrus	Bimodal	3	200	NA	NA	20	1.000	1.000	1.000	1.000
					Spherical, nonabsorbing, 0.12 μm					
Aerosol	Lognormal	0.001	0.75	0.06	1.7	0.12	1.000	1.000	1.000	1.000
					Spherical, nonabsorbing, 0.57 μm					
Aerosol	Lognormal	0.01	4	0.24	1.8	0.57	1.000	1.000	1.000	1.000
					Spherical, nonabsorbing, 1.28 μm					
Aerosol	Lognormal	0.01	8	0.5	1.85	1.28	1.000	1.000	1.000	1.000
					Spherical, nonabsorbing, 2.8 μm					
Aerosol	Lognormal	0.1	50	1	1.9	2.8	1.000	1.000	1.000	1.000

Table 1. (continued)

Type	Distribution Type	r_1(μm)	r_2(μm)	r_c(μm)	σ	r_e(μm)	SSA 446 nm	SSA 558 nm	SSA 672 nm	SSA 866 nm
				Spherical, SSA = 0.9, 0.12 μm						
Aerosol	Lognormal	0.003	0.75	0.06	1.7	0.12	0.910	0.900	0.885	0.853
				Spherical, SSA = 0.8, 0.12 μm						
Aerosol	Lognormal	0.003	0.75	0.06	1.7	0.12	0.821	0.800	0.774	0.720
				Medium dust						
Aerosol	Lognormal	0.1	1	0.5	1.5	0.75	0.920	0.977	0.995	0.997
				Large dust						
Aerosol	Lognormal	0.1	6	1	2	2.9	0.810	0.902	0.970	0.983

[a] r_1 and r_2 are the lower and upper radius limits of the aerosol distributions used to find the optical properties, respectively, r_c is the number median diameter of the lognormal size distributions, σ is the characteristic width of the lognormal size distributions, and r_e is the effective radius, (3/4)(V/S). Abbreviation is as follows: SSA, single-scattering albedo.

[24] Figure 2 shows MISR cirrus sensitivities for 12 simulated atmospheres. Each atmosphere contains a single crystal type, with particle size increasing systematically as one goes in columns from right to left (Baum D_e = 10, 40, 100, or 160 μm, respectively) and optical depth decreasing by row, from 0.5 at the top to 0.2 in the middle and then 0.05 at the bottom. χ^2_{max3} values are calculated for comparison atmospheres having optical depths ranging from 0 to 1 for all 18 Baum ice-crystal types. The Hex L/D = 2 types were included in the calculation but are not shown in Figure 2; their behavior is similar to the largest Baum crystal types. The blue areas in Figure 2 will generally be accepted, and all others rejected, based on the χ^2 tests. In all cases, MISR sensitivity to cirrus optical depth is within 0.05 or 20%, whichever is larger, similar to MISR aerosol optical depth sensitivity [*Kahn et al.*, 2001, 2005].

[25] Sensitivity to ice-crystal type is more complicated. When the simulated atmosphere contains Baum D_e = 10 μm crystals (left column in Figure 2), only Baum ice-crystal types having $D_e \leq 30$ μm are accepted. This is because the Baum D_e = 10 μm is dominated by droxtal-shaped crystals and the phase function generally increases with angle across range of MISR viewing angles (Figure 1). The Baum ice-crystal types having larger D_e contain significant fractions of other crystal shapes, generally hexagonal of some form, that greatly change the nature of the phase function. When the simulated atmosphere contains Baum D_e = 40 μm crystals (second column of Figure 2), the acceptance range is still quite small (20 μm $\leq D_e \leq$ 60 μm). The phase functions of the Baum crystal-types change with D_e greatly in this size range, corresponding to the change in the dominant crystal shape from droxtal to hexagonal types. When the simulated atmosphere contains Baum D_e = 100 and 160 μm crystals (third and fourth columns in Figure 2, respectively), the range of acceptable Baum D_e values is much wider (generally about 50 μm $\leq D_e \leq$ 180 μm). However, when D_e in the retrieval comparison space is larger than D_e in the simulated atmosphere, the retrieved optical depth is overpredicted by about 20% for those atmospheres having OD > 0.05. Smaller crystals are more efficient light scatterers, so there are corresponding optical depth underpredictions when the retrieved D_e is smaller than D_e in the atmosphere.

[26] To the extent that the 18 Baum ice-crystal types span the range of ice-crystal types found in the atmosphere, Figure 2 indicates that MISR aerosol retrievals would need to include between two and four ice-crystal types to capture this range. A large fraction of ice-crystal types in the atmosphere can be acceptably fit, to the degree of MISR sensitivity, with just two ice-crystal types, the small droxtal crystals (Baum D_e = 10–30 μm) and the larger crystals dominated by hexagonal shapes (Baum D_e = 100–160 μm). The retrieval space would be more complete if a third ice-crystal type were included to account for the transition between these two dominant shapes (e.g., Baum D_e = 40 μm). Even with three ice-crystal types in the retrieval, some overpredictions and underpredictions of cirrus optical depth would be expected if only one ice-crystal type is included for the larger, hexagonal crystals. In principle, an additional large crystal type could be included to help span this space and reduce optical depth errors.

2.4. MISR Theoretical Sensitivity to Cirrus Compared With Nonabsorbing Spheres

[27] In this and the following subsections, we explore the ability of MISR to discriminate between cirrus and aerosols. This subsection looks at cirrus and nonabsorbing spherical aerosols, whereas the next will address cirrus and large aerosols of various shapes. In both sections, we ask the following questions:

[28] 1. Might aerosols alone, or mixtures of ice crystals and aerosol types, be retrieved when only cirrus is actually present in the atmosphere? If so, how much of the cirrus optical depth can be falsely attributed to aerosol?

[29] 2. Conversely, might cirrus alone, or mixtures of cirrus and aerosols, be retrieved when only aerosols are present in the atmosphere? If so, how much of the total aerosol optical depth can be falsely attributed to cirrus?

[30] Ice crystals are nonspherical, generally nonabsorbing at visible wavelengths, and large compared to most aerosols. Many common aerosol types are not light absorbing, but differences in size, and, except for mineral dust, sphericity, produce phase function differences between cirrus and these aerosols that might be detected (Figure 1b). For this section, we defined five mixing groups, each containing three aerosol types and one crystal type. In each of the groups, the three aerosol types are 0.12 μm nonabsorbing spheres, 1.28 μm nonabsorbing spheres, and 2.8 μm nonabsorbing spheres (Table 1). The ice-crystal types vary across the five groups:

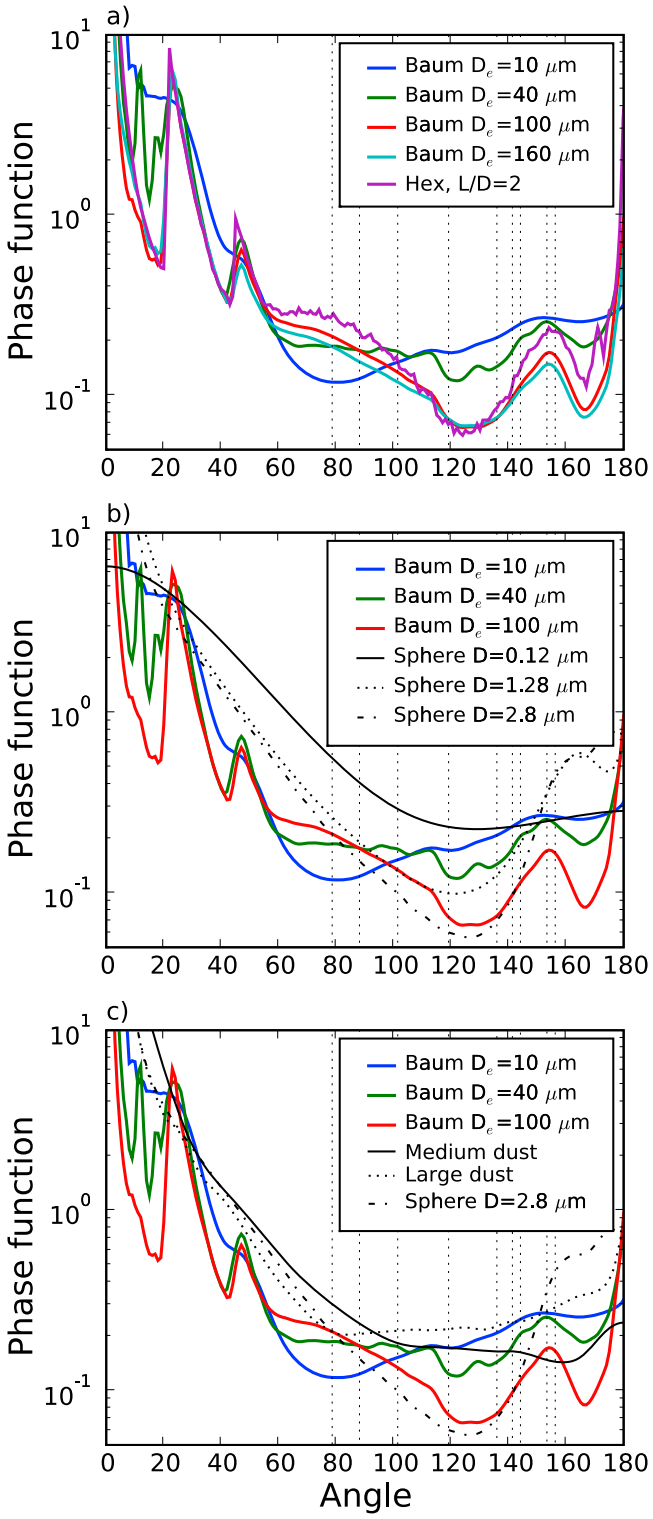

Figure 1. The phase functions at 672 nm, as functions of scattering angle, for (a) five ice-crystal types, (b) three ice-crystal types and three nonabsorbing particle types, and (c) three ice-crystal types and three large-particle types. The vertical dashed lines indicate the nine Multiangle Imaging Spectroradiometer (MISR) camera scattering angles at 10°S latitude at the equinox.

Baum D_e = 10, 40, 100, and 160 μm and Hex L/D = 2, respectively. The phase functions for these types are included in Figure 1b.

[31] In Figure 3 we test the ability of MISR to retrieve cirrus for simulated atmospheres that contain only cirrus. Each of the five mixing groups is represented by one column in Figure 3 and is tested against the simulated atmospheres. Four crystal types are used in the simulated atmospheres overall, represented by the four rows in Figure 3 (labeled along the right), each with three optical depths, which are shown as three bars. The height of each bar is the ratio of the optical depth for the retrieved comparison mixture having the lowest χ^2_{max3} to the optical depth of the atmosphere in that case. The width of each bar is inversely proportional to the best-fit χ^2_{max3} value, so wider bars represent more confident results. The fractional AOD contribution of each component is shown with color; cirrus components are blue, whereas aerosols are represented in other colors. In Figure 3, the wide bars where the blue portion extends to near a value of 1 are cases where cirrus was correctly identified as the component present, with approximately the correct optical depth. Wide bars that include large fractions of colors other than blue show conditions where aerosols were retrieved when only cirrus is in the atmosphere. Thin bars indicate that none of the comparison mixtures provided acceptable matches to the atmosphere. In Figure 3, thick blue bars from the lower left panel roughly along the diagonal to the two rightmost panels of the top row, and thin bars in all the off-diagonal panels, would represent perfect crystal-type versus aerosol discrimination.

[32] For the near-diagonal cases in Figure 3, the best-fit mixtures always match the atmospheric radiances well, and the correct total optical depth is retrieved. Cirrus correctly comprises most or all of the mixture in these cases, with increasing cirrus fraction for greater atmospheric optical depth. As we also found in Figure 2, the retrieval does not distinguish among the larger ice-crystal types. For example, when the ice-crystal type in the retrieval mixing group is Baum D_e = 100 μm and the simulated atmosphere contains Baum D_e = 160 μm (or vice versa), the best-fit mixtures are accepted and are mostly cirrus. In these retrievals, the Hex L/D = 2 ice-crystal type is also interchangeable with these large ice-crystal types, but with slightly lower cirrus optical depths. However, when the simulated atmosphere contains Baum D_e = 10 μm (bottom row of Figure 3), all crystal and aerosol types except the correct one are rejected, unless the optical depth is very low. This meets several retrieval expectations based on previous work: MISR sensitivity to particle properties increases with increased optical depth, and, due to a lack of spectral channels larger than 867 nm, discrimination among particle properties diminishes for particles larger than a few microns in size.

[33] In the MISR standard aerosol products up to version 22, all particle mixtures that meet the acceptance criteria are included in the calculation of "best-estimate" aerosol optical depth. As some of the accepted mixtures in Figure 3 include aerosols and retrieve total optical depths less than the atmospheric value, these cases would produce best-fit optical depth that could be skewed low, although the accepted cirrus mixtures would mitigate this effect. The reported best-fit optical properties, which are determined by the lowest-residual mixture, would correctly identify cirrus. Note also that in the off-diagonal panels in the upper left of Figure 3,

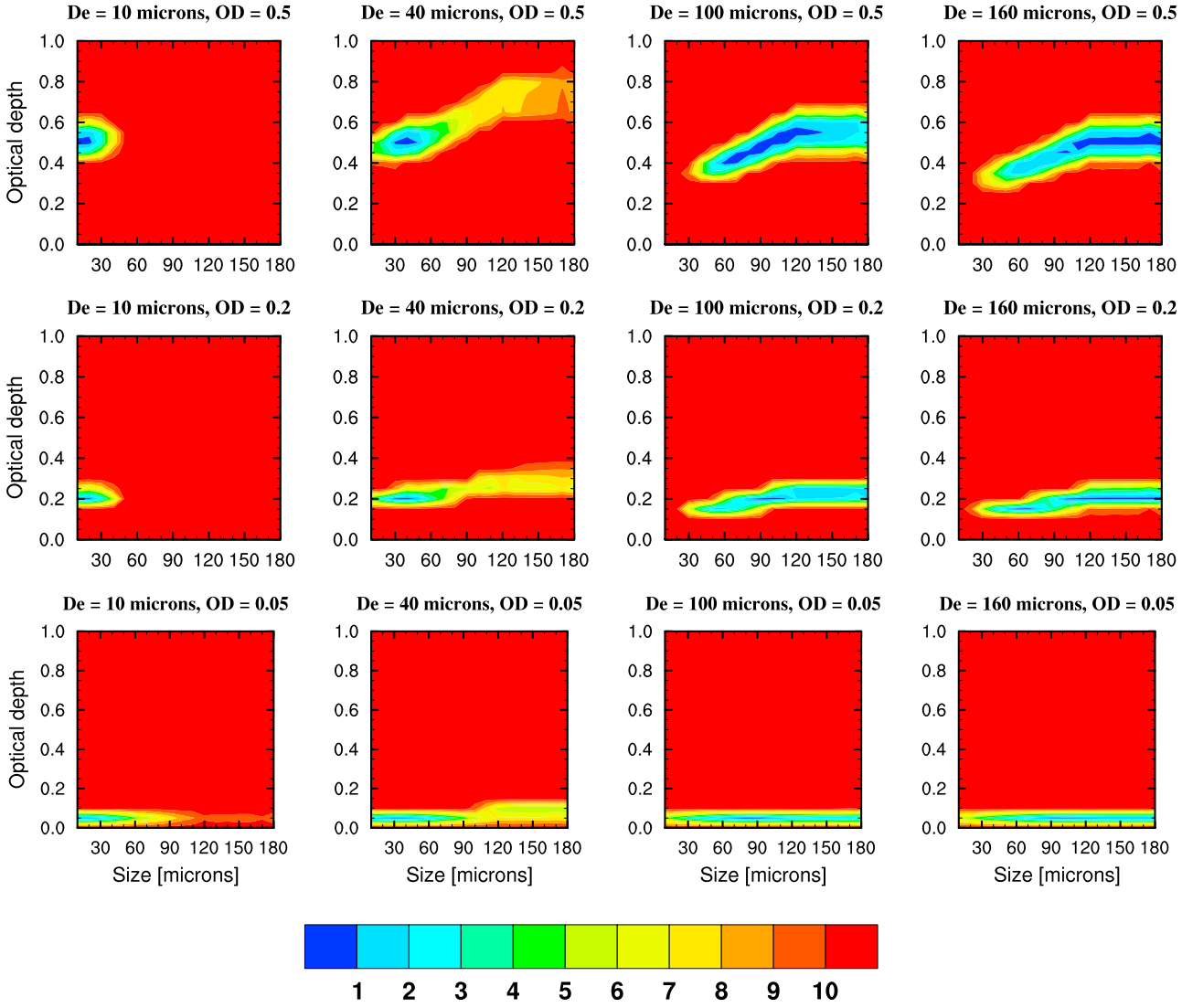

Figure 2. χ^2_{max3} as a function of retrieval optical depth and Baum-crystal effective diameter at 10°S at the equinox. For the simulated atmospheres, each column has a different ice-crystal type (left to right: Baum D_e = 10, 40, 100, 160 μm), and each row of panels has a different cirrus optical depth (top to bottom: 0.5, 0.2, 0.05).

when large (100 or 160 μm) crystals are in the atmosphere but the only crystals in the comparison space are 10 or 40 μm, the algorithm tends to favor large nonabsorbing spheres over the small crystals, but with decreasing confidence as the total optical depth increases.

[34] Figure 4 explores which mixtures fit best when the simulated atmosphere contains a single ice-crystal component but the MISR-retrieval comparison space contains no ice crystal and only three nonabsorbing spherical aerosols. Again, sensitivity to particle microphysical properties is low for low optical depth, except for the smallest ice crystals (Baum D_e = 10 μm), where all fits are rejected ($\chi^2_{max3} > 3$ for all cases). However, once the atmosphere contains at least 0.2 midvisible optical depth, the algorithm finds an acceptable match ($\chi^2_{max3} < 3$) only in the Baum D_e = 100 μm atmosphere case; all other cases correctly reject the available mixture options (i.e., no other fits are acceptable, as the χ^2_{max3} values all exceed 3). This finding is consistent with the initial tests of the MISR sensitivity to cirrus discussed by *Kahn et al.* [2001], that total column optical depth needs to be above about 0.2 to successfully distinguish between cirrus and aerosol.

[35] Figure 5 addresses the possibility of spherical aerosols being falsely attributed to cirrus. In these cases, the simulated atmosphere contains 2.8 μm (top row) or 0.12 μm (bottom row) spherical particles. The same five retrieval mixing groups used for Figure 3 are represented by the five columns here; however, the aerosol type in the simulated atmosphere is eliminated from the retrieval mixing group (e.g., for the top row, where the atmosphere contains 2.8 μm spheres, the comparison space mixing groups contain an ice-crystal type plus 1.28 μm spheres and 0.12 μm spheres only). In all cases, even the best fit is rejected. Nonabsorbing spheres cannot be fit with a combination of differently sized nonabsorbing spheres and cirrus under typical good observing conditions.

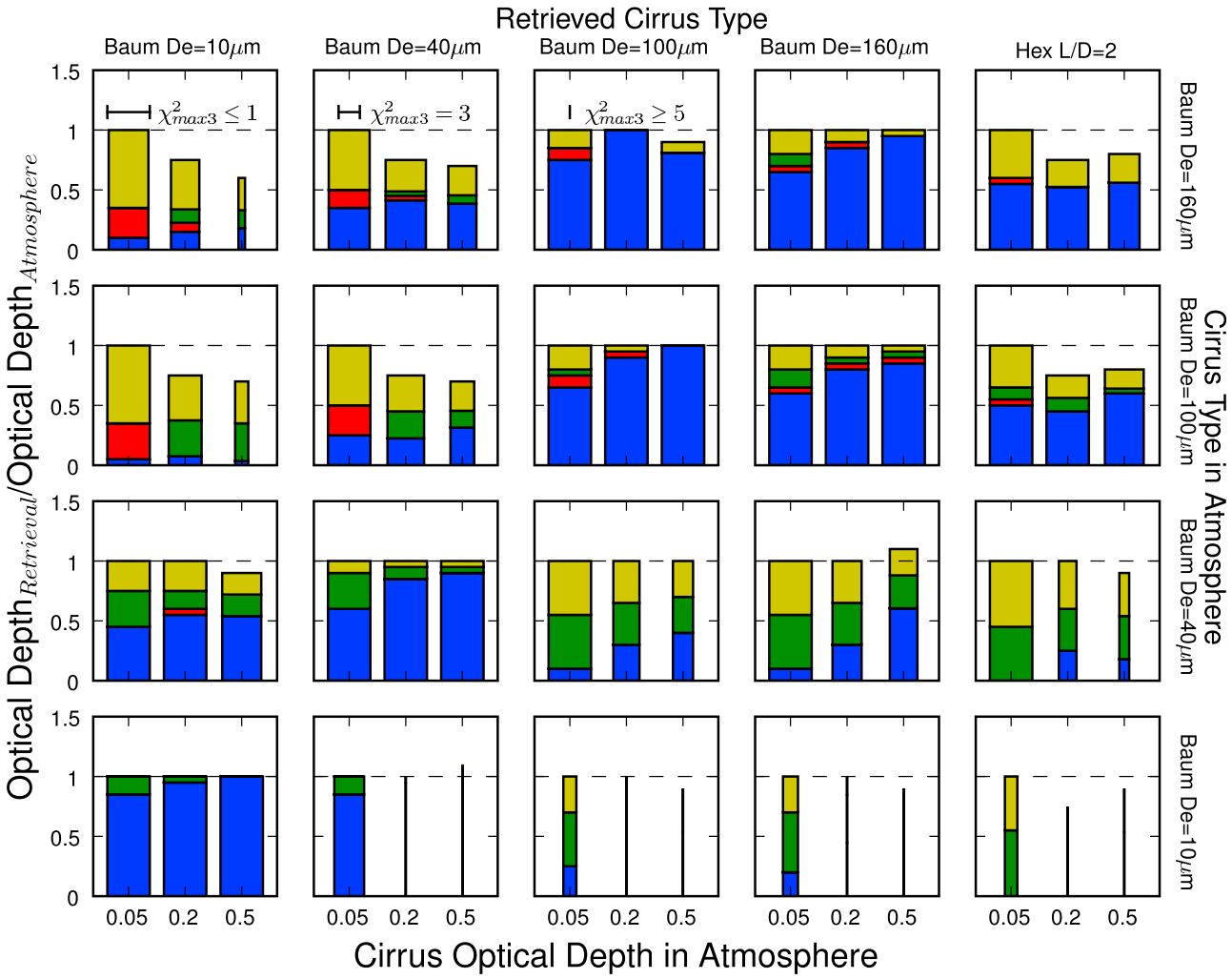

Figure 3. Sensitivity to cirrus atmospheres. Research algorithm aerosol retrieval results for simulated atmospheres containing only cirrus, for 10°S latitude equinox observing geometry, using aerosol mixing groups containing three sizes of nonabsorbing spheres and one ice-crystal type. The simulated atmospheres contain only cirrus: (row 1) Baum D_e = 160 μm, (row 2) Baum D_e = 100 μm, (row 3) Baum D_e = 40 μm, and (row 4) Baum D_e = 10 μm. Simulated atmosphere cirrus optical depths of 0.05, 0.2, and 0.5 are shown as the three bars. Lowest χ^2_{max3} results are shown for a mixing group containing 0.12 μm nonabsorbing spheres (yellow), 1.28 μm nonabsorbing spheres (green), 2.8 μm nonabsorbing spheres (red), and a ice-crystal type (blue). The cirrus types were varied among (column 1) Baum D_e = 10 μm, (column 2) Baum D_e = 40 μm, (column 3) Baum D_e = 100 μm, (column 4) Baum D_e = 160 μm, and (column 5) Hex L/D = 2. The height of each bar represents the ratio of retrieved to atmospheric optical depth for the best χ^2_{max3} case. The width of each bar is inversely proportional to χ^2_{max3} for values between 1 and 5. Cases where the best χ^2_{max3} is greater than 5 (poor fits) are represented as lines, and cases where the best χ^2_{max3} is less than 1 (good fits) are at full width.

2.5. MISR Theoretical Sensitivity to Cirrus Compared With Large and Nonspherical Aerosols

[36] In this section, we repeat the previous tests, but rather than retrieving cirrus with only nonabsorbing spheres, we consider dust and the largest of the nonabsorbing spheres from the previous section. Dust aerosol is potentially difficult to discriminate from cirrus because it is also nonspherical (albeit with different geometries), and even "medium dust" is generally large for an aerosol (Table 1). However, dust is somewhat absorbing at visible wavelengths, whereas ice crystals are not, which can help distinguish the two. The phase functions for the two dust types are plotted along with ice-crystal types and large nonabsorbing spheres in Figure 1c. These three aerosol types may be particularly difficult to distinguish from cirrus because their phase functions share characteristics with various ice-crystal types across the typical low-latitude MISR scattering angles. We again define five mixing groups having three aerosol types and one crystal type in each. In each group, the three aerosol types included are medium dust, large dust, and 2.8 μm nonabsorbing spheres. Again, each group also contains one of the five distinct ice-crystal types used previously.

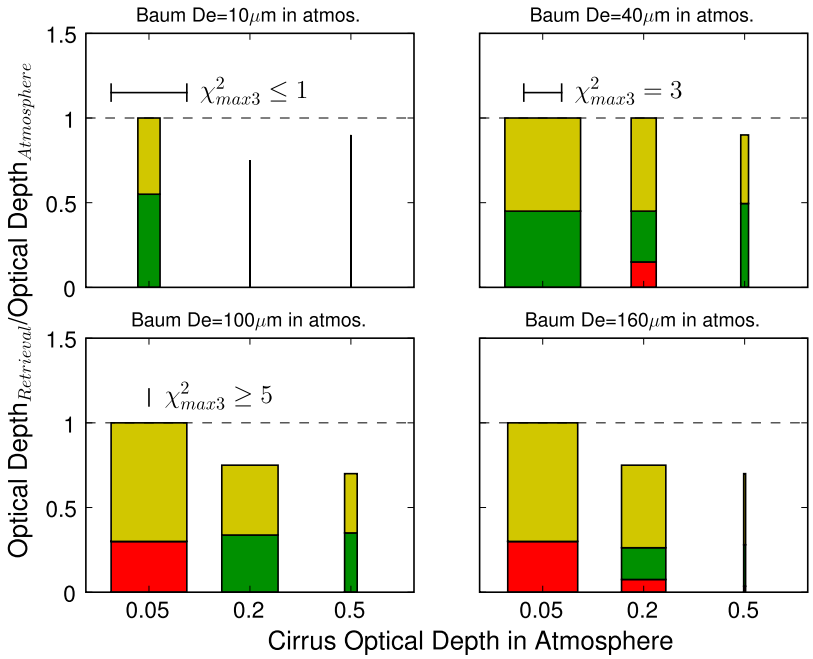

Figure 4. Retrieval results for atmospheres containing only cirrus when the retrieval algorithm comparison space contains only spherical, nonabsorbing particles of various sizes: 0.12 μm nonabsorbing spheres (yellow), 1.28 μm nonabsorbing spheres (green), and 2.8 μm nonabsorbing spheres (red). Simulated atmospheres contain D_e = 10, 40, 100, or 160 μm cirrus crystals, as indicated. Conventions for layout, bar thickness and height, and the simulated observing geometry are the same as those for Figure 3. Annotations above the dashed lines give the scale used to represent χ^2_{max3} values in all cases.

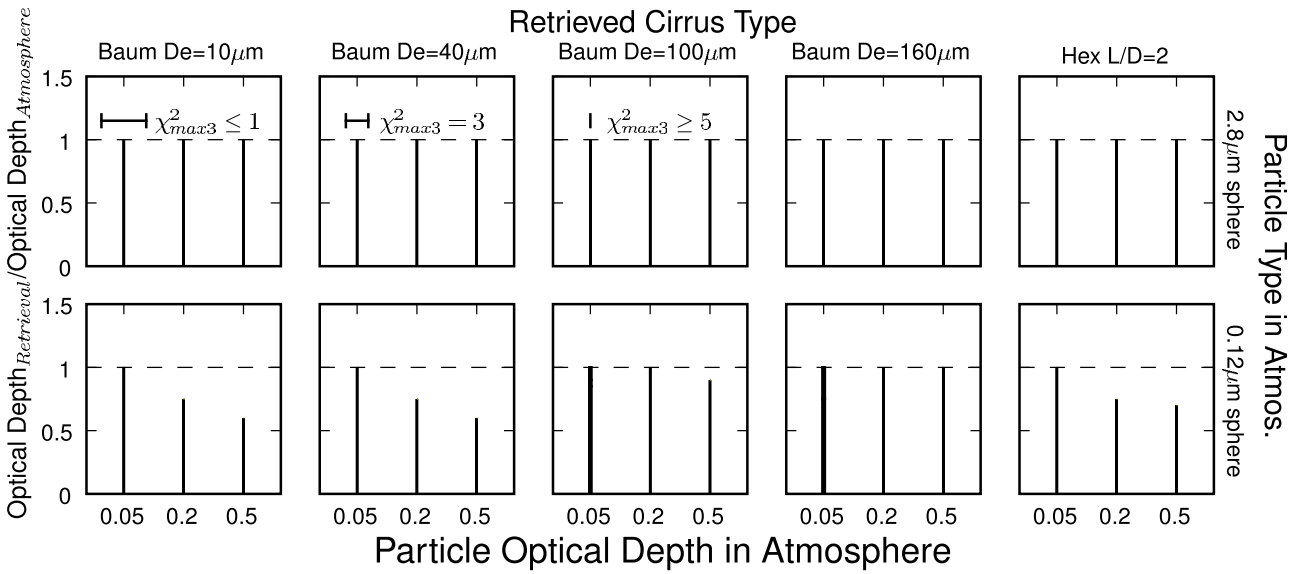

Figure 5. Testing the possibility that spherical aerosols can be falsely attributed to cirrus. For these tests, the simulated atmospheres contain only a single type of nonabsorbing sphere: (top) 2.8 μm or (bottom) 0.12 μm. The retrieval comparison space contains one ice-crystal component (blue), and two of the following three nonabsorbing spheres: 0.12 μm (yellow), 1.28 μm (green), and 2.8 μm (red); for each row, the nonabsorbing spherical particle type present in the simulated atmosphere is left out of the comparison space mixing group (e.g., the mixing group on the top row does not contain 2.8 μm spheres). Conventions for layout, bar thickness and height, comparison space ice-crystal component by column, and the simulated observing geometry are the same as those for Figure 3. As all cases are rejected, the bars are thin, and colors do not appear.

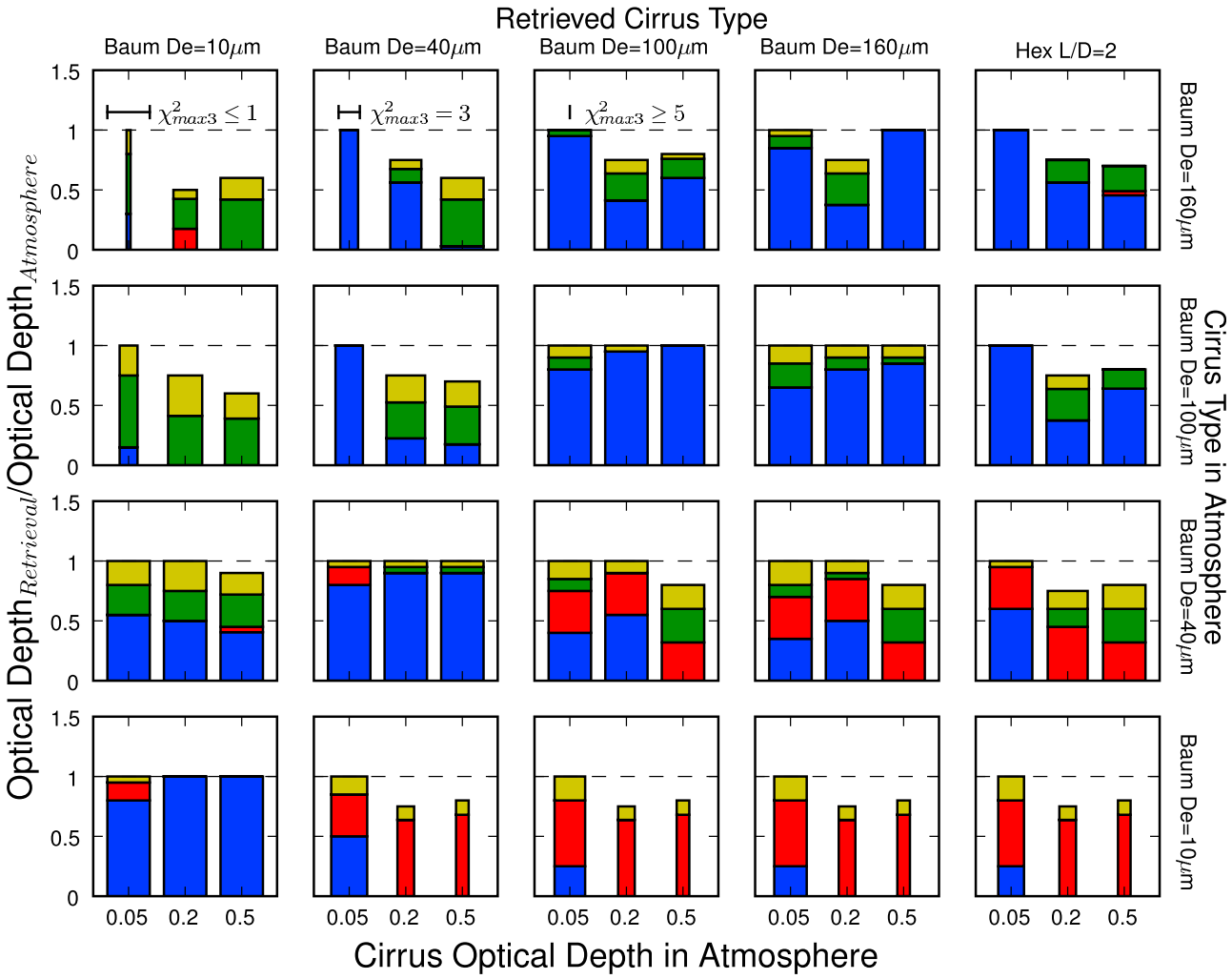

Figure 6. Testing the possibility that cirrus could be falsely identified as mineral dust or large spherical particles in simulated MISR retrievals. This figure is the same as Figure 3, except that in the comparison space mixing groups, the smaller nonabsorbing spheres have been replaced with mineral dust: cirrus (blue), 2.8 μm nonabsorbing spheres (yellow), medium dust (green), and large dust (red).

[37] In Figure 6 we test the ability of the MISR research retrieval to identify cirrus in simulated atmospheres that contain only cirrus. This figure is the same as Figure 3, except that the mixing groups in the retrieval comparison space contain dust instead of the smaller nonabsorbing spheres. As in Figure 3, along the near-diagonal from lower left to upper right, where the ice-crystal type in the retrieval mixing group matches the ice-crystal type in the atmosphere, the best-fit mixtures correctly contain cirrus and match the simulated observations well. Again the larger ice-crystal types (D_e = 100 and 160 μm, as well as Hex L/D = 2) are essentially indistinguishable in the MISR retrievals, the small crystals (D_e = 10 μm) are distinct except when the atmosphere has very low optical depth (fourth row of Figure 6), and the medium crystals (D_e = 40 μm) tend to be confused with aerosol particles when the comparison space does not contain medium crystals (third row of Figure 6). The observed ambiguity might be expected, as the phase functions for medium and large dust in Figure 1c are similar to that of Baum D_e = 40 μm throughout the range of MISR scattering angles at low latitudes.

[38] The retrieved total optical depths closely match those of the atmosphere in most cases when ice crystals are correctly retrieved as the particle type. However, in cases where large spherical or dust aerosol substitutes for cirrus in the retrieval result, total optical depth tends to be underestimated, especially as the atmospheric optical depth increases, and particle properties matter more to the result. These results indicate that for low-latitude geometry, combinations of large spherical aerosol and nonspherical mineral dust can be indistinguishable from the large ice-crystal types, and in such cases, the best-fit mixtures of aerosol and cirrus have only slightly lower χ^2_{max3} values than the component mixtures containing only cirrus that produce the correct optical depth.

[39] Especially with the reduced scattering angle coverage that occurs for low-latitude geometry, previous work indicated that there are limits to MISR particle type discrimination; these limitations are revealed by the current sensitivity study as well. For example, when the simulated atmosphere contains Baum D_e = 40 μm (third row of Figure 6), all retrievals that do not include this ice-crystal type tend to be accepted, but the best-fit fraction that is cirrus is always less

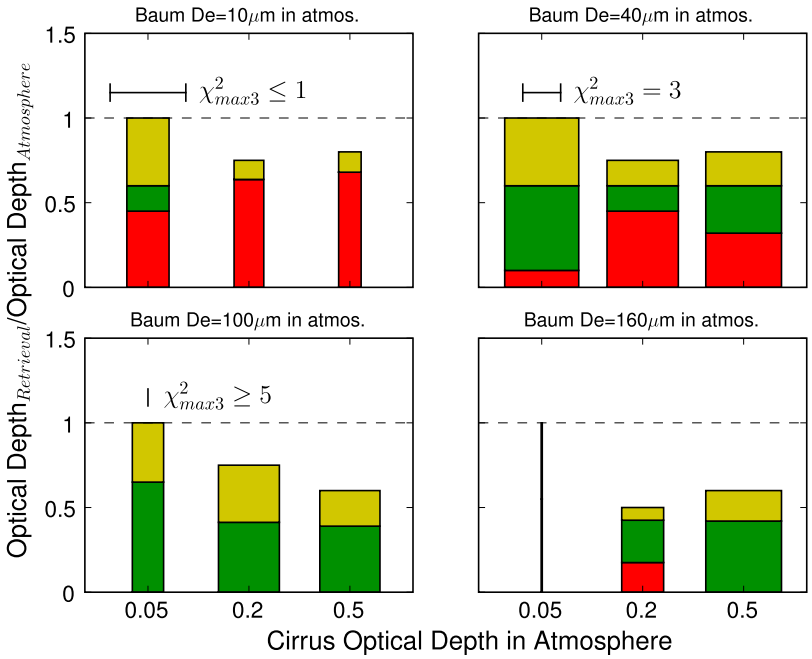

Figure 7. Retrieval results for atmospheres containing only cirrus when the retrieval algorithm comparison space contains only large spherical, nonabsorbing particles or dust: 2.8 μm nonabsorbing spheres (yellow), medium dust (green), and large dust (red). Simulated atmospheres contain D_e = 10, 40, 100, or 160 μm cirrus, as indicated. Conventions for layout, bar thickness and height, and the simulated observing geometry are the same as those for Figure 3.

than 0.6. The medium and large dust comprise a large fraction of these best fit mixtures, which makes sense considering that their phase functions are similar to that of Baum D_e = 40 μm throughout the range of MISR scattering angles (Figure 1c). However, at higher latitudes, MISR samples scattering angles smaller than 80°, approaching 40° near the poles; according to Figure 1c, we would expect greater distingishability between the cirrus and dust optical models away from the tropics.

[40] When the simulated atmosphere contains Baum D_e = 100 or 160 μm (top two rows of Figure 6), the retrieval mixing groups that contain Baum D_e = 10 or 40 μm tend to be rejected at low optical depths but are accepted at higher optical depths, and the results contain very little cirrus. This behavior is different from typical MISR-sensitivity results, where sensitivity to particle properties increases with increasing atmospheric optical depth. It occurs in this case because a mixture of about two-thirds medium dust and one-third large spheres happens to match the large ice-crystal signal when the combined aerosol optical depth is about 60% of the cirrus optical depth. The total optical depth in the MISR research retrieval is evaluated in steps of 0.05, so in the case when the cirrus optical depth in the atmosphere is 0.05, the MISR research retrieval does not evaluate the total optical depth of 0.03 where the combination of medium dust and large spheres would give a good fit. Conversely, when the cirrus optical depth in the atmosphere is 0.5, the MISR research retrieval does evaluate the total optical depth of 0.3 and has a good fit. This decreased sensitivity at higher optical depths for combinations of dust and large spheres misrepresenting cirrus also occurs, although to a lesser degree, at midlatitudes (40°N tested, but not shown). However, the sensitivity of MISR to cirrus generally increased overall at 40°N, as expected.

[41] Figure 7 explores which mixtures fit best when the atmosphere contains a single ice-crystal component whereas the MISR-retrieval comparison space contains no ice-crystal components and does contain one large nonabsorbing spherical component and two dust components (similar to Figure 4, but focusing now on larger and nonspherical particles). Each of the four simulated-atmosphere cases again contains one of four ice-crystal types. The results here parallel those for the off-diagonal panels in Figure 6, discussed above. The Baum De = 10 μm crystals tend to be distinct (i.e., no acceptable cases with $\chi^2_{\text{max3}} < 3$), but for the other atmospheres, the match improves (χ^2_{max3} decreases), and the optical depth decreases, as large spheres and dust are indistinguishable from the larger crystals. In light of the results presented earlier, this is not surprising, but it raises a caution about retrievals in dusty marine regions that contain dust, sea salt (which can be large, spherical particles) and cirrus.

[42] As in the previous subsection, we also need to determine if these large aerosol types can be mistaken for cirrus or mixtures of cirrus and other large aerosol types. In Figure 8, the simulated atmospheres contain either large dust (top row) or medium dust (bottom row). The five retrieval mixing groups from Figure 3 are represented by the five columns. Again, the aerosol type actually contained in the simulated atmosphere is eliminated from the retrieval comparison space (e.g., for the top row, where the atmosphere contains large dust, the mixing groups contain only an ice-crystal type, 2.8 μm spheres, and medium dust). Acceptable fits of the simulated atmosphere containing large dust occur for the larger optical depths in the retrievals with mixing groups

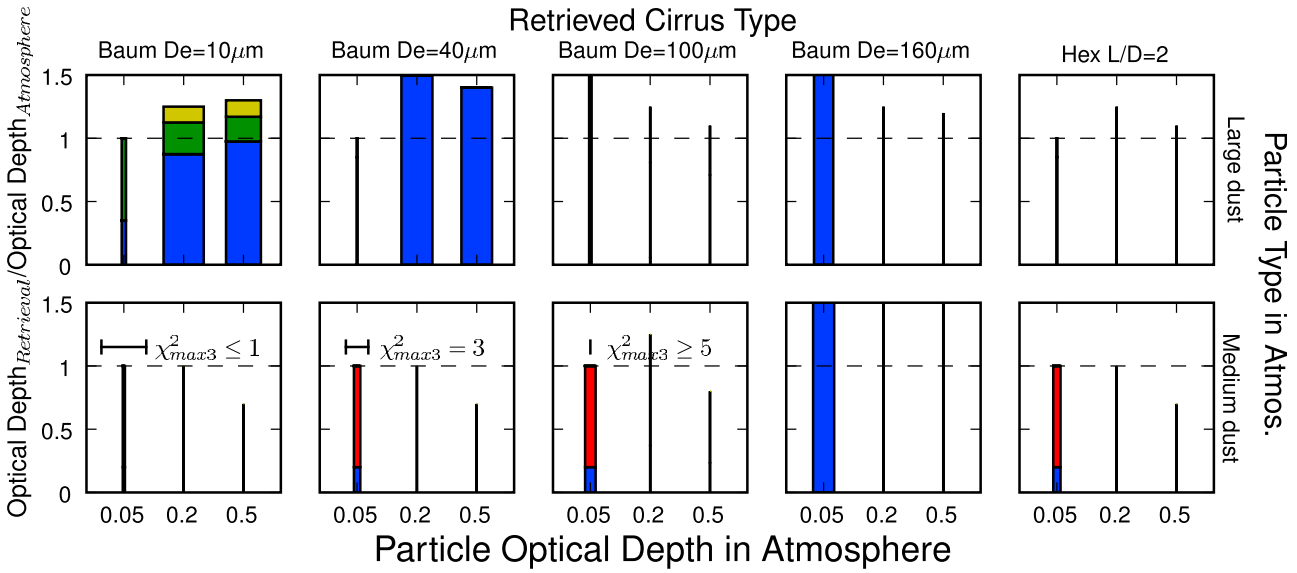

Figure 8. Testing the possibility that dust aerosol can be falsely attributed to cirrus. For these tests, the simulated atmospheres contain only (top) large dust or (bottom) medium dust. The retrieval comparison space contains one cirrus component (blue), the 2.8 μm nonabsorbing sphere component (yellow), and one of the two nonspherical dust components, medium dust (green) or large dust (red); for each row, the particle type present in the simulated atmosphere is left out of the mixing group (e.g., the mixing group on the top row does not contain large dust). Conventions for layout, bar thickness and height, comparison space cirrus component by column, and the simulated observing geometry are the same as those for Figure 3.

containing Baum D_e = 10 or 40 μm. In these cases, the retrieved mixtures are primarily cirrus, and the total optical depths are greater than that of the dust in the atmosphere; that is, when cirrus substitutes for aerosol, the optical depth can be overestimated. In all other cases, there are no acceptable matches when the comparison space does not contain the particles in the simulated atmosphere. However, the cases where large dust may be misattributed to cirrus again highlight the limitations for distinguishing cirrus and aerosols in dusty marine environments.

3. Comparison of MISR Cirrus and Aerosol Retrievals With Ground-Based Lidar and Aerosol Robotic Network

[43] We now investigate MISR's ability to retrieve cirrus in natural settings by testing MISR retrievals coincident with ground-based MicroPulse Lidar located at the Department of Energy's Atmospheric Radiation Measurement Climate Research Facilities located in the tropical western Pacific and AERONET data. Information about the 42 test cases is given in Table 2, which covers a range of cirrus optical depths from 0 to about 0.3. The first letter of each case name represents its location, either Manus, Papua New Guinea (M), Darwin, Australia (D), or Nauru (N). The second letter indicates whether the case has a lidar-derived cirrus optical depth, with optical depths between 0.03 and 0.3 (C), an AERONET aerosol optical depth (only the highest-quality level 2.0 data are used) (A), or both (B). Unfortunately, there were only six cases where the lidar-derived cirrus optical depths are between 0.03 and 0.3 and AERONET also retrieved a level 2.0 aerosol optical depth (lower-quality level 1.5 data did not provide additional cases here). This lack of coincident optical depth measurements is because AERONET aerosol optical depth is screened for cloud contamination. Cirrus optical depths from the lidar are retrieved using the lidar transmittance method described by *Comstock and Sassen* [2001]. Lidar optical depths were retrieved using backscatter profiles averaged over 5 min to improve the signal-to-noise ratio, and lidar backscatter was visually inspected to verify cloud boundaries and presence of aerosol.

[44] The mean and standard deviations of cirrus optical depths were found using data from 15 min before until 15 min after the MISR overpass. Mean aerosol optical depths from AERONET were also found using data from this same time span (standard deviation not given because there were at most two measurements in this time interval).

[45] For each case listed in Table 2, MISR research aerosol retrievals were attempted for between 3 and 14 different 3 km × 3 km patches within ~200 km of the lidar stations. Patches were chosen manually by viewing the true-color images from the nine MISR cameras and checking digitally for scene homogeneity between the cameras. Closer patches were given preference; however, sometimes distance from the surface site was required to obtain a successful retrieval, due primarily to scene variability, as discussed below. Table 2 shows the number of retrieval patches tested as well as the number of successful patches, for which at least one cirrus/aerosol mixture was retrieved having $\chi^2_{\mathrm{max3}} < 3$. On some days when thin cirrus clouds were measured, a large number of patches were needed to assess the cirrus field variability. (Note that for many cases, the standard deviations in optical depth measured by lidar are as large as the mean.) Consistent with this interpretation, fewer patches were generally required to obtain successful retrievals in situations where cirrus clouds were absent. On some days when thin cirrus

Table 2. Information on Coincident Lidar-Multiangle Imaging Spectroradiometer and Coincident Aerosol Robotic Network-Multiangle Imaging Spectroradiometer Retrievals[a]

Case Name, Location	Date, YMD[b]	MISR Time	MISR Orbit	MISR Path	Lidar cirrus OD (STD)[c]	AERONET OD[d]	Patches attempted	Patches successful
MC1. Manus[e]	2000-03-23	0053	1393	97	0.2 (0.09)	NA	10	5
MC2. Manus[e]	2000-04-08	0053	1626	97	0.13 (0.16)	NA	14	4
MC3. Manus[e]	2000-10-10	0046	4320	96	0.16 (0.21)	NA	10	4
DC1. Darwin[f]	2005-03-29	0136	28072	105	0.17 (0.1)	NA	3	0
DC2. Darwin[f]	2006-01-27	0136	32499	105	0.26 (0.32)	NA	3	0
DC3. Darwin[f]	2006-02-12	0136	32732	105	0.26 (0.29)	NA	3	3
DC4. Darwin[f]	2006-02-19	0142	32834	106	0.1 (0.11)	NA	4	2
DC5. Darwin[f]	2006-03-07	0142	33067	106	0.1 (0.11)	NA	7	6
DC6. Darwin[f]	2006-04-15	0148	33635	107	0.2 (0.284)	NA	5	2
DC7. Darwin[f]	2006-05-19	0136	34130	105	0.14 (0.16)	NA	6	2
DC8. Darwin[f]	2006-06-27	0142	34698	106	0.16 (0.08)	NA	7	1
DC9. Darwin[f]	2007-07-16	0143	40290	106	0.09 (0.07)	NA	11	6
DB1. Darwin[f]	2005-07-26	0142	29805	106	0.08 (0.09)	0.08	6	1
DB2. Darwin[f]	2005-09-03	0149	30373	107	0.05 (0.05)	0.32	9	7
DB3. Darwin[f]	2005-09-21	0136	30635	105	0.06 (0.09)	0.33	7	7
DA1. Darwin[f]	2005-06-08	0142	29106	106	0.0 (0.0)	0.15	6	3
DA2. Darwin[f]	2005-06-24	0142	29339	106	0.0 (0.0)	0.17	4	2
DA3. Darwin[f]	2005-08-04	0136	29936	105	0.0 (0.0)	0.17	3	3
DA4. Darwin[f]	2005-08-11	0142	30038	106	0.0 (0.0)	0.14	4	3
DA5. Darwin[f]	2005-08-18	0149	30140	107	0.0 (0.0)	0.14	5	5
DA6. Darwin[f]	2005-08-20	0136	30169	105	0.02 (0.04)	0.16	4	2
DA7. Darwin[f]	2005-09-28	0142	30737	106	0.0 (0.0)	0.33	5	5
DA8. Darwin[f]	2007-10-27	0149	41790	107	0.0 (0.0)	0.24	4	3
DA9. Darwin[f]	2007-11-28	0149	42256	107	0.0 (0.0)	0.27	3	3
DA10. Darwin[f]	2007-11-30	0136	42285	105	0.0 (0.0)	0.15	3	2
NC1. Nauru[g]	2000-11-29	2336	5062	85	0.06 (0.03)	NA	8	5
NC2. Nauru[g]	2001-06-02	2326	7756	84	0.05 (0.05)	NA	6	4
NC3. Nauru[g]	2001-10-08	2323	9620	84	0.1 (0.11)	NA	7	4
NC4. Nauru[g]	2005-12-22	2326	31988	84	0.22 (0.34)	NA	4	2
NC5. Nauru[g]	2006-07-11	2320	34915	83	0.16 (0.08)	NA	7	4
NC6. Nauru[g]	2007-02-20	2321	38177	83	0.07 (0.09)	NA	7	3
NB1. Nauru[g]	2005-06-20	2333	29294	85	0.05 (0.07)	0.12	9	9
NB2. Nauru[g]	2005-06-29	2327	29425	84	0.08 (0.09)	0.15	8	3
NB3. Nauru[g]	2007-03-08	2321	38410	83	0.03 (0.04)	0.12	8	4
NA1. Nauru[g]	2005-03-18	2321	27925	83	0.0 (0.01)	0.09	5	4
NA2. Nauru[g]	2005-09-01	2326	30357	84	0.0 (0.0)	0.08	5	4
NA3. Nauru[g]	2006-04-13	2326	33619	84	0.0 (0.0)	0.09	6	3
NA4. Nauru[g]	2007-02-18	2333	38148	85	0.0 (0.0)	0.09	3	1
NA5. Nauru[g]	2007-06-28	2321	40041	83	0.0 (0.0)	0.08	3	3
NA6. Nauru[g]	2007-09-14	2333	41177	85	0.0 (0.0)	0.09	3	3
NA7. Nauru[g]	2007-09-30	2333	41410	85	0.01 (0.02)	0.15	4	4
NA8. Nauru[g]	2007-10-25	2327	41774	84	0.0 (0.0)	0.09	3	3
NA9. Nauru[g]	2007-11-26	2327	42240	84	0.0 (0.0)	0.09	4	4

[a]Definitions are as follows: AERONET, Aerosol Robotic Network, MISR, Multiangle Imaging Spectroradiometer; OD, optical depth.
[b]YMD is year, month, day; for example, read 2000-03-23 as 23 March 2000.
[c]Mean and SD values for cirrus OD are found using lidar data from 15 min before to 15 min after the MISR overpass.
[d]AERONET OD is the mean value of measurements taken from 15 min before to 15 min after the MISR overpass.
[e]Latitude = 2.06°S, longitude = 147.43°E.
[f]Latitude = 12.42°S, longitude = 130.89°E.
[g]Latitude = 0.52°S, longitude = 166.90°E.

were measured by the lidar, only a few patches were found where we judged that a MISR retrieval might be successful (e.g., DC1 and DC2), so no more than several patches were attempted, and in these two cases, none of the patches resulted in successful retrieval fits). The 16 mixing groups listed in Table 3, each containing one ice-crystal type plus three aerosol types, were all tested for each patch. Large nonabsorbing spheres and medium dust are included in each mixing group because sea-salt aerosols are common at these maritime sites, and the sites also occasionally receive transported dust [*Kahn et al.*, 2001] (transported dust tends to be depleted of larger dust particles). The third aerosol component in each mixing group is varied among the small nonabsorbing sphere, two small absorbing spheres having two different single-scattering albedo values, and a medium nonabsorbing sphere. These account for the possibility that transported biomass burning, pollution aerosol, or a smaller mode of sea-salt aerosol is present. The same vertical distributions of cirrus and aerosol assumed in the MISR research retrieval described in section 2.2 are used here.

[46] To assess the ability of MISR to retrieve cirrus when cirrus are present, Figure 9a shows the results of the coincident lidar- and MISR-retrieved cirrus optical depth comparisons for days where the lidar detected thin cirrus (OD between 0.03 and 0.3). For each case, the blue circle shows the mean lidar-retrieved optical depth, and the blue line shows the standard deviation due to cirrus variability. The red symbols show the cirrus optical depth for the best-fit mixture

Table 3. Multiangle Imaging Spectroradiometer Research Retrieval Mixing Groups Used for Comparison to Lidar and Aerosol Robotic Network[a]

Mixing Group	Cirrus-Crystal Type	Particle Type 1	Particle Type 2	Particle Type 3
1	Baum D_e = 10 μm	Spherical, nonabs, 0.12 μm	Spherical, nonabs, 2.8 μm	Medium dust
2	Baum D_e = 10 μm	Spherical, SSA = 0.9, 0.12 μm	Spherical, nonabs, 2.8 μm	Medium dust
3	Baum D_e = 10 μm	Spherical, SSA = 0.8, 0.12 μm	Spherical, nonabs, 2.8 μm	Medium dust
4	Baum D_e = 10 μm	Spherical, nonabs, 0.57 μm	Spherical, nonabs, 2.8 μm	Medium dust
5	Baum D_e = 40 μm	Spherical, nonabs, 0.12 μm	Spherical, nonabs, 2.8 μm	Medium dust
6	Baum D_e = 40 μm	Spherical, SSA = 0.9, 0.12 μm	Spherical, nonabs, 2.8 μm	Medium dust
7	Baum D_e = 40 μm	Spherical, SSA = 0.8, 0.12 μm	Spherical, nonabs, 2.8 μm	Medium dust
8	Baum D_e = 40 μm	Spherical, nonabs, 0.57 μm	Spherical, nonabs, 2.8 μm	Medium dust
9	Baum D_e = 100 μm	Spherical, nonabs, 0.12 μm	Spherical, nonabs, 2.8 μm	Medium dust
10	Baum D_e = 100 μm	Spherical, SSA = 0.9, 0.12 μm	Spherical, nonabs, 2.8 μm	Medium dust
11	Baum D_e = 100 μm	Spherical, SSA = 0.8, 0.12 μm	Spherical, nonabs, 2.8 μm	Medium dust
12	Baum D_e = 100 μm	Spherical, nonabs, 0.57 μm	Spherical, nonabs, 2.8 μm	Medium dust
13	Hex, L/D = 2	Spherical, nonabs, 0.12 μm	Spherical, nonabs, 2.8 μm	Medium dust
14	Hex, L/D = 2	Spherical, SSA = 0.9, 0.12 μm	Spherical, nonabs, 2.8 μm	Medium dust
15	Hex, L/D = 2	Spherical, SSA = 0.8, 0.12 μm	Spherical, nonabs, 2.8 μm	Medium dust
16	Hex, L/D = 2	Spherical, nonabs, 0.57 μm	Spherical, nonabs, 2.8 μm	Medium dust

[a]Abbreviations are as follows: nonabs, nonabsorbing; SSA, single-scattering albedo.

of each patch, provided $\chi^2_{max3} < 3$ for the best-fit mixture. The shapes of the symbols denote the ice-crystal type in the mixing group having the best fit. The wide pink bars give the range of MISR-retrieved cirrus optical depths from any acceptable fit from all patches considered. The cases are arranged in order of lowest to highest lidar-retrieved mean cirrus OD.

[47] In 70% of the 24 cases in Figure 9a, MISR obtains good agreement with the lidar-retrieved OD. To be classified as good agreement (1) the mean lidar-retrieved cirrus OD must be within the span of accepted MISR cirrus fits and (2) a majority of the MISR best-fit cirrus optical depths must fall within one standard deviation of the lidar cirrus optical depth. Of the 7 cases that did not meet both the mean and standard deviation criteria above, 2 cases had no acceptable fits (DC1 and DC2), 4 had MISR biased significantly low (DC3, DC8, DB1, and NC5), and in 1, MISR was biased significantly high (DB2).

[48] In this limited sample, MISR tends to be biased low more often than high; about nine cases appear to be biased low (including cases classified as good fits) versus three that appear to be biased high. The low bias is more prevalent when the lidar-retrieved cirrus OD is higher and has greater variability (right-hand side of Figure 9a). Horizontal inhomogeneity in the cirrus field probably contributes to the low bias, combined with several attributes of the way MISR aerosol retrievals are performed; Figure 10 illustrates the point. Because cirrus clouds in the tropical region tend to be 10–15 km above the surface, the cirrus appear to move over 50 km relative to Earth's surface between the most oblique forward and aft MISR cameras. For inhomogeneous cirrus fields, thicker cirrus may appear in a given surface location for one camera, whereas thin cirrus or no cirrus at all may appear above the same surface location when viewed by other cameras. This relative movement between cameras is used to retrieve the heights and wind speeds of optically thick clouds and aerosol plumes [*Moroney et al.*, 2002; *Marchand et al.*, 2007; *Kahn et al.*, 2007]; however, the low optical depths of thin cirrus clouds are often below the cloud-screening detection limit. The MISR standard aerosol retrievals used to generate MISR aerosol products are based on the assumption of aerosol homogeneity over a 17.6 km aerosol retrieval region and the requirement that a significant fraction of 1.1 km subregions within the retrieval region meet angle-to-angle smoothness and angle-to-angle correlation criteria. Data are filtered for these criteria automatically by the MISR standard aerosol retrieval algorithm [*Martonchik et al.*, 2009; *Kahn et al.*, 2009]. For the research aerosol retrieval algorithm used here, such tests are done by hand. Variability is more likely to be significant, and to be detected and screened out by both methods, when the optical depth of the scene is higher, producing a statistically net low bias to the MISR retrievals. Furthermore, even if this variability is not entirely screened out, it will contribute to noise in the data and will cause χ^2_{max3} values to increase. This will reduce the number of successful retrievals for high and highly variable OD cases and contribute to a low bias in the MISR optical depth retrievals.

[49] The mixing groups having the best fits in the various patches studied here predominantly contain the Baum D_e = 10 or 20 μm crystal types (67% of the time, shown by red crosses in Figure 9a). This result indicates that MISR finds that these high, thin cirrus clouds often have the scattering properties of droxtal crystals, a result consistent with measurements showing that such crystals are common in high cirrus clouds [*Zhang et al.*, 2004]. However, as we do not have additional information on the actual crystal types for these cirrus, it is difficult to evaluate further MISR's ability to discriminate ice-crystal shape.

[50] To assess the ability of MISR to retrieve little or no cirrus on days when no cirrus are present according to the lidar measurements, Figure 9b shows the comparison of lidar-retrieved cirrus optical depths with MISR-retrieved cirrus optical depths for the cases where the lidar-retrieved cirrus optical depth was less than 0.03. Only two patches had best-fit cirrus optical depths above 0.1 across all cases, and only two cases had any acceptable fits with cirrus optical depths above 0.2. These results are consistent with the theoretical studies in this paper; under most conditions, the best-fit retrievals will not falsely attribute aerosol to cirrus. In several cases (e.g., DA9, DA10, and NA7), the best-fit retrievals do show thin cirrus with optical depths >0.05 for some patches. This may be due to (1) the presence of large dust aerosols, (2) some combination of aerosol types that can be mistaken

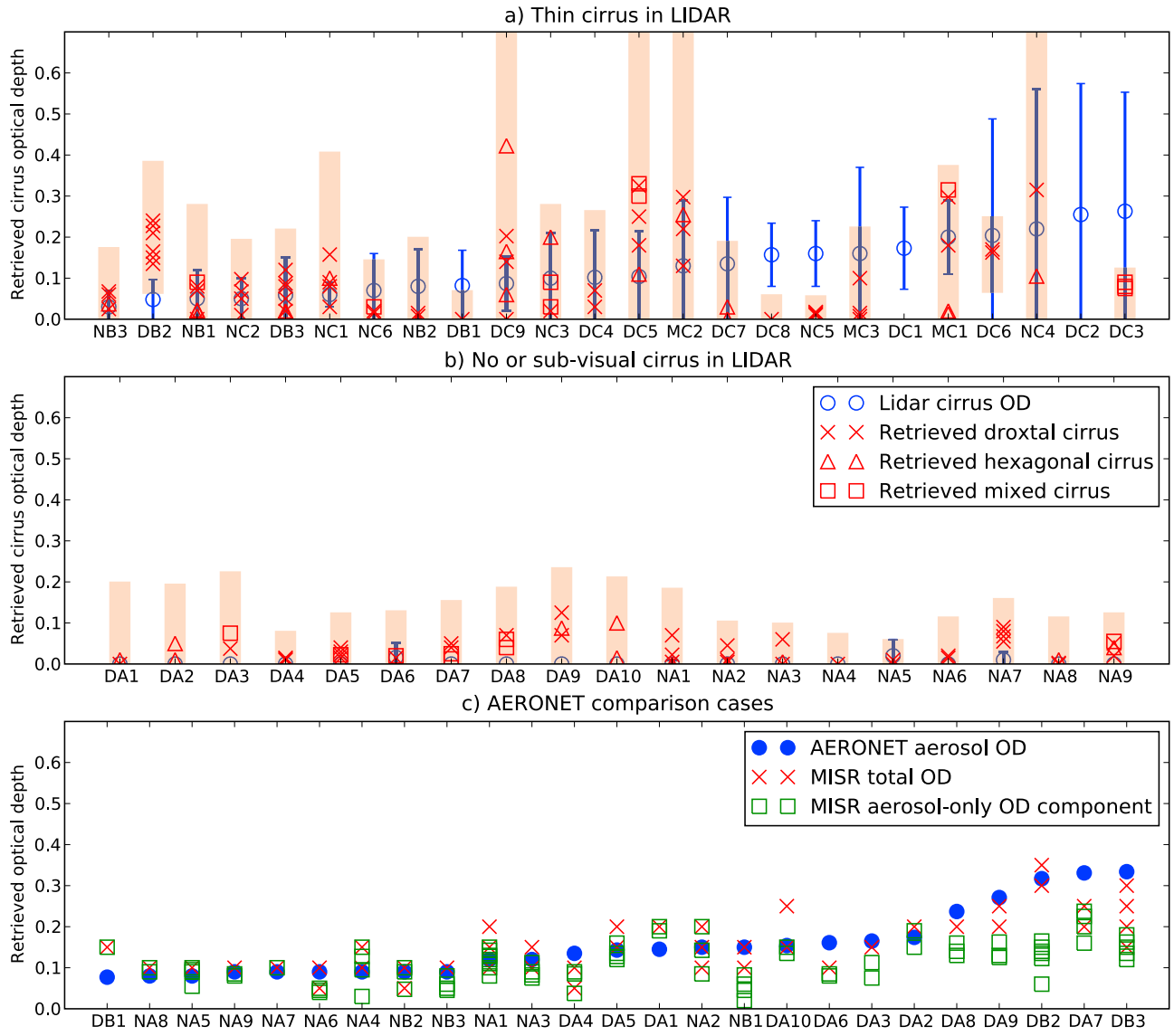

Figure 9. (a) Cirrus optical depths (ODs) retrieved by lidar and MISR for all coretrieved lidar/MISR cases where the mean lidar cirrus optical depths are between 0.03 and 0.3. The blue circles show the mean lidar-retrieved cirrus optical depth, averaged over 30 min centered on the MISR overpass; blue error bars represent the cirrus optical depth standard deviation for this period. The cases are arranged in order of lowest to highest lidar-retrieved mean cirrus OD. The red crosses, triangles, and squares represent the MISR-retrieved cirrus optical depths for patches having the lowest χ^2_{max3} values near the lidar site. (Only patches for which $\chi^2_{max3} < 3$ are included here.) Crosses represent cases where best-fit cirrus were dominated by droxtal shapes, and triangles where they were dominated by hexagonal crystal shapes; squares are for mixed cirrus-shape results. The red bars represent the range of MISR-retrieved cirrus optical depths for all successful patches in the region. (b) Same as Figure 10a, except for cases where lidar cirrus optical depths are less than 0.03. Since all lidar-retrieved cirrus optical depths are very low, the cases are arranged in chronological order by site. (c) Comparison of optical depths measured by Aerosol Robotic Network (AERONET) and MISR. Blue circles show AERONET optical depths, red crosses show the best-fit total (aerosol plus cirrus) optical depths that passed the acceptance criterion ($\chi^2_{max3} < 3$) from any patch, and green squares show the best-fit aerosol-only optical depths that passed the acceptance criterion. The cases are arranged in order of lowest to highest AERONET-retrieved aerosol OD.

for cirrus, or (3) the actual presence of cirrus that did not pass directly over the lidar station within 15 min of the MISR overpass but was within the MISR swath. Due to scene variability, the third possibility is especially likely in many cases.

[51] Figure 9c shows a comparison between AERONET-retrieved AOD and best-fit MISR-retrieved OD, arranged in order of increasing AERONET AOD. Included are both the MISR-retrieved total (cirrus plus aerosol) OD and MISR-

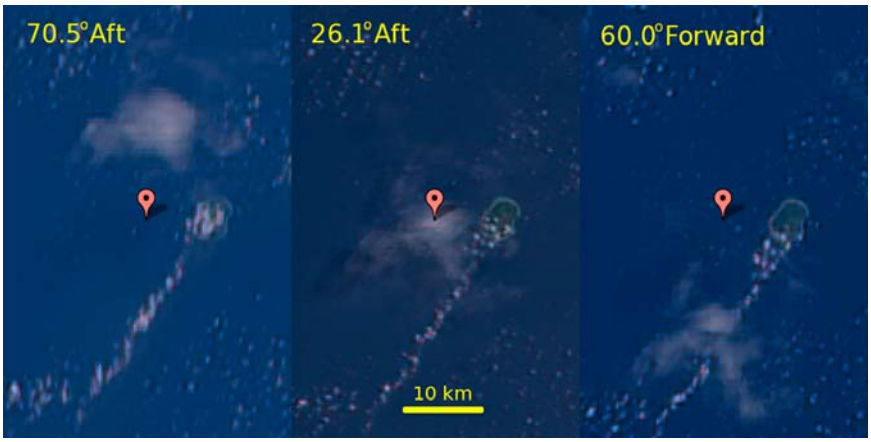

Figure 10. Demonstration of the relative movement of small-spatial-scale cirrus compared to the surface when viewed from three different MISR cameras (parallax). Images were taken from orbit 27896 off the coast of Nauru Island. The red marker identifies a stationary point on the surface. When viewed from different angles, the cirrus cloud appears to move relative to the surface.

retrieved aerosol-only OD for successful patches near the AERONET site. The AERONET/MISR comparison shows generally good results for both the MISR total OD and the MISR aerosol-only OD at low OD (OD < 0.2, left side of Figure 9c); however, at higher OD (OD > 0.2, right side of Figure 9c), the MISR total OD compares better with AERONET than the MISR aerosol-only OD, which is generally lower. There are only a few instances in all cases where the MISR total OD is significantly higher than the AERONET AOD. Overall the retrieval of total optical depth is very good, with a correlation coefficient of 0.83 and a mean normalized bias of −2.5% (biased low). Because of the disagreement at high AERONET AOD, the comparison to MISR aerosol-only OD was not as strong, having a correlation coefficient of 0.56 and a mean normalized bias of −26% (biased low); again the leading cause seems likely to be scene variability. However, we note that the very small number of validation cases within the scope of the present study does not in itself address the ability of MISR to retrieve total and aerosol-only OD in the presence of cirrus globally.

[52] For the high AERONET AOD cases, there are two possible explanations as to why the MISR total OD agrees with the AERONET AOD but the MISR aerosol-only OD does not: (1) there could actually be cirrus in the atmosphere that is not filtered out by the AERONET cloud-screening process and (2) MISR might be falsely attributing some aerosol optical depth to cirrus. A combination of these explanations is likely occurring, as is shown by exploring individual cases. For the cases NB1, DB2, and DB3, Figure 9a shows that cirrus is measured in the atmosphere by the lidar and is also detected by MISR. In these three cases, it appears to be most likely that AERONET AOD contains cirrus OD to some degree, and the AOD reported by AERONET is actually AERONET aerosol plus cirrus OD. (Note: For case DB2, the MISR cirrus OD is higher, so both explanations may apply here.) Conversely, cases DA3, DA8, DA9, and DA7 had little to no cirrus measured by the lidar, whereas MISR did retrieve at least some cirrus (Figure 9b). In these cases, it appears more likely that either aerosol is being falsely attributed to cirrus by MISR or that there was cirrus near the measurement site observed by MISR and AERONET but not by the lidar. Regardless of the explanation, the results in Figure 9c show that MISR retrieves total (aerosol plus cirrus) optical depth with high reliability in the presence of thin cirrus.

[53] More evaluation of MISR's ability to discriminate between aerosols and thin cirrus must be done to validate a global thin cirrus product. Future implementation would benefit from using 3-D global chemical-transport models to determine if dust or cirrus is likely to be present in a MISR retrieval region.

4. Conclusions

[54] In this paper we explored the sensitivity of MISR aerosol retrievals to thin cirrus clouds, both theoretically and using observations from ground-based lidar and AERONET. In the theoretical tests of atmospheres containing only cirrus, we found that MISR is sensitive to cirrus optical depth within Max{0.05, 20%}, similar to the sensitivity of MISR to aerosol optical depth, provided the retrieval comparison space contains a good match to ice-crystal type in the atmosphere. MISR can distinguish between small, droxtal-like ice crystals and larger, hexagonal-like crystals based on single-scattering phase function differences, even at low latitudes, where MISR does not sample scattering angles below about 80°. However, in situations where cirrus is present but the retrieval comparison space lacks these components, the retrieval tends to underestimate OD, especially for OD greater than 0.1.

[55] Cirrus generally cannot be mistaken for combinations of nonabsorbing spherical aerosols when the cirrus optical depth is greater than about 0.2. However, we found several cases where cirrus can be mistaken for combinations of dust and large spheres (and visa versa), even at optical depths of 0.5, for low-latitude geometries, where the range of scattering angles observed by MISR is smallest.

[56] In comparisons with near-coincident lidar observations, MISR successfully retrieved cirrus optical depth in 70% of cases (criteria defined in section 3). However, the ability to test MISR optical depth retrievals in situations of higher cirrus optical depth (OD > 0.15) was limited due to scene variability. Horizontally inhomogeneous fields of very

thin cirrus provide inherent difficulties for the MISR retrieval approach, and, in addition, differences between the MISR and ground-truth observation coverage regions can be important. In cases where little to no cirrus were detected by the lidar, MISR best fits did not attribute more than 0.05 OD to cirrus in most cases.

[57] MISR total OD compared well to AERONET AOD (correlation coefficient of 0.83 and a mean normalized bias of −2.5%); however, MISR aerosol-only OD was often lower than AERONET AOD in cases where the AERONET AOD was greater than 0.2. This is most likely due to cirrus in the atmosphere that is not filtered out of the AERONET AOD product or MISR falsely attributing some AOD as cirrus OD. Individual cases show that a combination of these explanations is likely.

[58] The results of this paper show that MISR standard aerosol retrievals could be improved by the inclusion of between two and four ice-crystal types in the standard-algorithm comparison space to complement the existing eight aerosol types. Due to computational limitations of the algorithm, adding two ice-crystal types may be the most practical, and would capture typical MISR sensitivity to the natural range of cirrus properties in most situations. On the basis of the results presented here, these would include one small, droxtal-like crystal type (e.g., Baum D_e = 10 μm) and one larger, hexagonal-like crystal type (e.g., Baum D_e = 100 μm). At least two crystal types are needed because of the large differences in the associated phase functions between the droxtal-like and hexagonal-like types at the wavelengths and scattering angles observed by MISR. The cirrus optical models used here were derived primarily from available in situ aircraft measurements. To the extent that they represent the range of natural conditions, they establish the degree of generality of our approach. However, the ice-crystal models we use assume smooth crystal surfaces and no entrained air bubbles, so sensitivity to cirrus might change somewhat for next-generation cirrus optical models that account for these features [*Yang et al.*, 2008]. It is also possible that the ice crystals in thin cirrus may have effective diameters smaller than 10 μm [*Lin et al.*, 1998], which is the smallest effective diameter tested here, and this may also affect the sensitivity. In addition, a basic assumption in the MISR standard aerosol retrieval algorithm is spatial homogeneity on 10 km scales. As expected, and as illustrated by the validation examples of section 3, this assumption is frequently violated in regions where cirrus is commonly observed; a practical implementation of thin cirrus retrieval in the MISR standard aerosol algorithm over water should probably include an initial assessment of scene spatial variability on these scales.

[59] The ability to distinguish between aerosols and thin cirrus by a multiangle, multispectral satellite instrument can be increased by including wavelengths longer than the 0.867 μm MISR band (e.g., 1.6 μm) or by including polarization measurements. A quantitative assessment of how aerosol/cirrus sensitivity would be improved by these additions would be important for future mission design.

[60] **Acknowledgments.** We thank our colleagues on the Jet Propulsion Laboratory's MISR instrument team and at the NASA Langley Research Center's Atmospheric Sciences Data Center for their roles in producing the MISR data sets. We also thank Michael Garay at the Jet Propulsion Laboratory for contributions to early work on MISR cirrus sensitivity, Brian Baum at the University of Wisconsin-Madison for developing the cirrus optical models used here, Zibo Zhang at the NASA Goddard Space Flight Center for helpful discussions, and the AERONET principal investigators for contributing to the global aerosol database. J.P. was funded by a NASA Postdoctoral Fellowship for this work. R.K. is supported in part by NASA's Climate and Radiation Research and Analysis Program, under H. Maring, NASA's Atmospheric Composition Program, and the EOS-MISR project. Contributions from J.C. were supported by NASA NEWS and Department of Energy's Atmospheric Radiation Measurement programs.

References

Baum, B., A. Heymsfield, P. Yang, and S. Bedka (2005a), Bulk scattering properties for the remote sensing of ice clouds: Part I. Microphysical data and models, *J. Appl. Meteorol.*, *44*(12), 1885–1895, doi:10.1175/JAM2308.1.

Baum, B., P. Yang, A. Heymsfield, S. Platnick, M. King, Y. Hu, and S. Bedka (2005b), Bulk scattering properties for the remote sensing of ice clouds: Part II. Narrowband models, *J. Appl. Meteorol.*, *44*(12), 1896–1911, doi:10.1175/JAM2309.1.

Chen, W.-T., R. A. Kahn, D. Nelson, K. Yau, and J. H. Seinfeld (2008), Sensitivity of multiangle imaging to the optical and microphysical properties of biomass burning aerosols, *J. Geophys. Res.*, *113*, D10203, doi:10.1029/2007JD009414.

Comstock, J. M., and K. Sassen (2001), Retrieval of cirrus cloud radiative and backscattering properties using combined lidar and infrared radiometer (LIRAD) measurements, *J. Atmos. Oceanic Technol.*, *18*(10), 1658–1673.

Comstock, J., T. Ackerman, and G. Mace (2002), Ground-based lidar and radar remote sensing of tropical cirrus clouds at Nauru Island: Cloud statistics and radiative impacts, *J. Geophys. Res.*, *107*(D23), 4714, doi:10.1029/2002JD002203.

Dessler, A. E., and P. Yang (2003), The distribution of tropical thin cirrus clouds inferred from terra MODIS data, *J. Clim.*, *16*(8), 1241–1247.

Dessler, A. E., S. P. Palm, W. D. Hart, and J. D. Spinhirne (2006), Tropopause-level thin cirrus coverage revealed by ICESat/Geoscience Laser Altimeter System, *J. Geophys. Res.*, *111*, D08203, doi:10.1029/2005JD006586.

Diner, D., et al. (1998), Multi-angle Imaging SpectroRadiometer (MISR): Instrument description and experiment overview, *IEEE Trans. Geosci. Remote Sens.*, *36*(4), 1072–1087, doi:10.1109/36.700992.

Forster, P., et al. (2007), Changes in atmospheric constituents and in radiative forcing, in *Climate Change 2007: The Physical Science Basis. Contribution of Working Group I to the Fourth Assessment Report of the Intergovernmental Panel on Climate Change*, edited by S. Solomon et al., pp. 129–234, Cambridge Univ. Press, New York.

Grant, I., and G. Hunt (1968), Solution of radiative transfer problems using invariant SN method, *Mon. Not. R. Astron. Soc.*, *141*(1), 27–41.

Immler, F., K. Krueger, S. Tegtmeier, M. Fujiwara, P. Fortuin, G. Verver, and O. Schrems (2007), Cirrus clouds, humidity, and dehydration in the tropical tropopause layer observed at Paramaribo, Suriname (5.8°N, 55.2°W), *J. Geophys. Res.*, *112*, D03209, doi:10.1029/2006JD007440.

Kahn, R., R. West, D. McDonald, B. Rheingans, and M. Mishchenko (1997), Sensitivity of multiangle remote sensing observations to aerosol sphericity, *J. Geophys. Res.*, *102*(D14), 16,861–16,870, doi:10.1029/96JD01934.

Kahn, R., P. Banerjee, D. McDonald, and D. Diner (1998), Sensitivity of multiangle imaging to aerosol optical depth and to pure-particle size distribution and composition over ocean, *J. Geophys. Res.*, *103*(D24), 32,195–32,213, doi:10.1029/98JD01752.

Kahn, R., P. Banerjee, and D. McDonald (2001), Sensitivity of multiangle imaging to natural mixtures of aerosols over ocean, *J. Geophys. Res.*, *106*(D16), 18,219–18,238, doi:10.1029/2000JD900497.

Kahn, R., B. Gaitley, J. Martonchik, D. Diner, K. Crean, and B. Holben (2005), Multiangle Imaging Spectroradiometer (MISR) global aerosol optical depth validation based on 2 years of coincident Aerosol Robotic Network (AERONET) observations, *J. Geophys. Res.*, *110*, D10S04, doi:10.1029/2004JD004706.

Kahn, R. A., W.-H. Li, C. Moroney, D. J. Diner, J. V. Martonchik, and E. Fishbein (2007), Aerosol source plume physical characteristics from space-based multiangle imaging, *J. Geophys. Res.*, *112*, D11205, doi:10.1029/2006JD007647.

Kahn, B. H., C. K. Liang, A. Eldering, A. Gettelman, Q. Yue, and K. N. Liou (2008), Tropical thin cirrus and relative humidity observed by the Atmospheric Infrared Sounder, *Atmos. Chem. Phys.*, *8*(6), 1501–1518.

Kahn, R. A., D. L. Nelson, M. Garay, R. C. Levy, M. A. Bull, D. J. Diner, J. V. Martonchik, S. R. Paradise, E. G. Hansen, and L. A. Remer (2009), MISR aerosol product attributes, and statistical comparisons with MODIS, *IEEE Trans. Geosci. Remote Sens.*, *47*(12), 4095–4114, doi:10.1109/TGRS.2009.2023115.

Kalashnikova, O., and R. Kahn (2006), Ability of multiangle remote sensing observations to identify and distinguish mineral dust types: 2. Sensitivity over dark water, *J. Geophys. Res.*, *111*, D11207, doi:10.1029/2005JD006756.

Kaufman, Y., et al. (2005), A critical examination of the residual cloud contamination and diurnal sampling effects on MODIS estimates of aerosol over ocean, *IEEE Trans. Geosci. Remote Sens.*, *43*(12), 2886–2897, doi:10.1109/TGRS.2005.858430.

Lin, H., K. J. Noone, J. Strom, and A. J. Heymsfield (1998), Small ice crystals in cirrus clouds: A model study and comparison with in situ observations, *J. Atmos. Sci.*, *55*, 1928–1939.

Macke, A., J. Mueller, and E. Raschke (1996), Single scattering properties of atmospheric ice crystals, *J. Atmos. Sci.*, *53*, 2813–2825, doi:10.1175/1520-0469(1996)053<2813:SSPOAI>2.0.CO;2.

Marchand, R. T., T. P. Ackerman, and C. Moroney (2007), An assessment of Multiangle Imaging Spectroradiometer (MISR) stereo-derived cloud top heights and cloud top winds using ground-based radar, lidar, and microwave radiometers, *J. Geophys. Res.*, *112*, D06204, doi:10.1029/2006JD007091.

Martonchik, J., D. Diner, R. Kahn, T. Ackerman, M. Verstraete, B. Pinty, and H. Gordon (1998), Techniques for the retrieval of aerosol properties over land and ocean using multiangle imaging, *IEEE Trans. Geosci. Remote Sens.*, *36*(4), 1212–1227, doi:10.1109/36.701027.

Martonchik, J. V., R. A. Kahn, and D. J. Diner (2009), Retrieval of aerosol properties over land using MISR observations, in *Satellite Aerosol Remote Sensing Over Land*, edited by A. A. Kokhanovsky and G. de Leeuw, pp. 267–294, Springer, Berlin.

McFarlane, S. A., and R. T. Marchand (2008), Analysis of ice crystal habits derived from MISR and MODIS observations over the ARM Southern Great Plains site, *J. Geophys. Res.*, *113*, D07209, doi:10.1029/2007JD009191.

McFarlane, S. A., R. T. Marchand, and T. P. Ackerman (2005), Retrieval of cloud phase and crystal habit from Multiangle Imaging Spectroradiometer (MISR) and Moderate Resolution Imaging Spectroradiometer (MODIS) data, *J. Geophys. Res.*, *110*, D14201, doi:10.1029/2004JD004831.

Mishchenko, M., W. Rossow, A. Macke, and A. Lacis (1996), Sensitivity of cirrus cloud albedo, bidirectional reflectance and optical thickness retrieval accuracy to ice particle shape, *J. Geophys. Res.*, *101*(D12), 16,973–16,985, doi:10.1029/96JD01155.

Moroney, C., R. Davies, and J.-P. Muller (2002), Operational retrieval of cloud-top heights using MISR data, *IEEE Trans. Geosci. Remote Sens.*, *40*(7), 1532–1540, doi:10.1109/TGRS.2002.801150.

Sassen, K., and B. Cho (1992), Subvisual thin cirrus lidar dataset for satellite verification and climatological research, *J. Appl. Meteorol.*, *31*(11), 1275–1285, doi:10.1175/1520-0450(1992)031<1275:STCLDF>2.0.CO;2.

Takano, Y., and K. Liou (1989), Solar radiative-transfer in cirrus clouds: 1. Single-scattering and optical-properties of hexagonal ice crystals, *J. Atmos. Sci.*, *46*, 3–19, doi:10.1175/1520-0469(1989)046<0003:SRTICC>2.0.CO;2.

Yang, P., G. Hong, G. W. Kattawar, P. Minnis, and Y. Hu (2008), Uncertainties associated with the surface texture of ice particles in satellite-based retrieval of cirrus clouds: Part II. Effect of particle surface roughness on retrieved cloud optical thickness and effective particle size, *IEEE Trans. Geosci. Remote Sens.*, *46*(7), 1948–1957, doi:10.1109/TGRS.2008.916472.

Zhang, Z., P. Yang, G. Kattawar, S. Tsay, B. Baum, Y. Hu, A. Heymsfield, and J. Reichardt (2004), Geometrical-optics solution to light scattering by droxtal ice crystals, *Appl. Opt.*, *43*(12), 2490–2499, doi:10.1364/AO.43.002490.

Zhao, G. (2006), Cloud observations from EOS-Terra: From conception to interpretation of cloud climatologies with a focus on small clouds, Ph.D. thesis, 117 pp., Univ. of Ill., Urbana-Champaign.

Zhao, G., and L. Di Girolamo (2004), A cloud fraction versus view angle technique for automatic in-scene evaluation of the MISR cloud mask, *J. Appl. Meteorol.*, *43*(6), 860–869, doi:10.1175/1520-0450(2004)043<0860:ACFVVA>2.0.CO;2.

J. M. Comstock, Pacific Northwest National Laboratory, Richland, WA 99352, USA.

M. R. Davis, Science Systems and Applications, Inc., Lanham, MD 20706, USA.

R. A. Kahn, Laboratory for Atmospheres, NASA Goddard Space Flight Center, Greenbelt, MD 20771, USA. (ralph.kahn@nasa.gov)

J. R. Pierce, Department of Physics and Atmospheric Science, Dalhousie University, Halifax, NS B3H 3J5, Canada.